E-25-633

FINAL REPORT
NASA GRANT NSG-3106

SURFACE TEMPERATURES AND GLASSY STATE INVESTIGATIONS IN TRIBOLOGY

Co-Principal Investigators
S. Bair, Research Engineer
W. O. Winer, Professor

Prepared for

NASA-LEWIS RESEARCH CENTER
21000 Brookpark Road
Cleveland, Ohio 44135

July 1982

GEORGIA INSTITUTE OF TECHNOLOGY
A UNIT OF THE UNIVERSITY SYSTEM OF GEORGIA
SCHOOL OF MECHANICAL ENGINEERING
ATLANTA, GEORGIA 30332

1982

GEORGIA INSTITUTE OF TECHNOLOGY
SCHOOL OF MECHANICAL ENGINEERING
ATLANTA, GEORGIA 30332

SURFACE TEMPERATURES AND GLASSY STATE INVESTIGATIONS IN TRIBOLOGY

NASA GRANT
NSG-3106

Co-Principal Investigators

S. Bair
Research Engineer

W. O. Winer
Professor

for

NASA-Lewis Research Center
21000 Brookpark Road
Cleveland, Ohio 44135

June 1982

GEORGIA INSTITUTE OF TECHNOLOGY
SCHOOL OF MECHANICAL ENGINEERING
ATLANTA, GEORGIA 30332

SURFACE TEMPERATURES AND GLASSY STATE INVESTIGATIONS IN TRIBOLOGY

Ward O. Winer, Ph.D.
Professor
Principal Investigator

Scott Bair
Research Engineer
Principal Investigator

June 1982

ABSTRACT

This is the fifth and final annual report covering the period July 1980 - October 1981 of NASA Grant NSG-3106 and deals only with the research performed over that period. Preliminary measurements of high shear rate viscosity at near atmospheric but variable pressure suggest the importance of low normal stress and cavitation or fluid fracture in the type of stress field existing in elastohydrodynamic inlets and classical hydrodynamic configurations. An experimental basis is given for three regimes of traction in concentrated contacts: a thin film regime characterized by high traction and determined by lambda ratio, a thick film regime characterized by low traction and determined by the speed parameter, and the elastohydrodynamic regime for which traction is controlled by limiting shear stress. Traction measurements were performed with various liquids, two solid lubricants, and a grease. Film thickness and traction measurements of polymer blends and base oils are compared.

TABLE OF CONTENTS

LIST OF TABLES

LIST OF ILLUSTRATIONS

Figure Page

INTRODUCTION

Although this is a final report, it consists only of research performed during the final year of the grant. Previous reports were self-contained in content and are merely referenced [1,2,3,4]. The research during this past year mainly consisted of a) high shear rate viscometry at near atmospheric pressure, b) traction regimes studies in elastohydrodynamic contacts with Newtonian lubricants, c) traction measurements with various non-Newtonian liquid lubricants, a grease and two solid lubricants, and d) elastohydrodynamic film thickness measurements with polymer blends and base oils. In addition, two sets of measurements were performed at the request of the contract monitor on materials supplied. Copies of letters documenting these results are included in this report as Appendix A and B.

The focus of the research continued to be on the mechanics of behavior of lubricants in concentrated contacts both with respect to the film thickness and traction behavior as well as the rheological behavior of the lubricants.

The lubricant rheology studies were preliminary high shear stress-shear rate measurements near atmospheric pressure to explore the role of principle normal stress and material fracture in non-Newtonian rheology of lubricants. The tentative conclusion of this work is that the pseudoplastic behavior of some liquids is apparently the result of the reduction of the principle normal stress at high shear stress causing void formation and the reduction of apparent viscosity. These results, if verified, may have serious implications with respect to lubricant feed at high shear rates in both elasto-hydrodynamic and hydrodynamic lubrication. They also supplement the high pressure limiting shear stress rheological model developed by the authors. This work should be pursued more thoroughly.

The concentrated contact mechanics studies reported make a significant contribution to the understanding of the regimes of traction behavior in elastohydrodynamic lubrication as distinct from the film thickness regimes. The elastohydrodynamic film thickness measurements with polymer blends and base oils illustrate that the presence of polymers does cause an increase in film thickness but not to the extent that would be expected from low shear rate viscosity measurements of the polymer blend.

The experimental equipment used in this year's research consists of the concentrated contact simulator, the constant pressure stress-strain apparatus, and a rotary viscometer. The latter was constructed during this contract year and is described below while the others are described in previous reports [1,2].

HIGH SHEAR RATE VISCOMETRY

Nonlinear effects in the measurement of liquid lubricant viscosity at atmospheric pressure are familiar in the literature [5-8]. One may speculate that these effects are occurring at the onset of a limiting shear stress. If so, high shear rate viscometry at low pressure could be used to extend to lower pressure the limiting shear stress-pressure data already generated at high pressures [1,2,3].

However, for some high shear rate viscosity data at atmospheric pressure the principle normal stress may approach quite low values relative to one atmosphere suggesting the possibility of cavitation or fracture of the material resulting in a reduced shear stress. Viscosity measurements at varying pressures near atmospheric pressure should be able to distinguish between these two mechanisms. If the controlling mechanism is related to a limiting shear stress in the material, modest (0.1 to 10 bar) changes in pressure should have little influence. However if the mechanism is associated with fracture due to changing normal stress, these modest changes in atmospheric pressure should have a significant effect on the measured viscosity. Preliminary measurements suggest the later mechanism.

Equipment

The rotary viscometer (Figure 1) is of the concentric cylinder type and with the use of various cylinder sets, a shear stress to 300 kPa and a shear rate of 12,000 s^{-1} can be reached. In addition, the viscometer is sealed to allow internal air pressures to be varied from subambient 10 kPa to 1 MPa (e.g., 0.1 to 10 bar). The internal cylinder is driven through a flexible shaft by a constant velocity motor and ten speed gear box. The torque sensor consists of a frame which deflects at one end a distance proportional to the torque at the large cylinder. The frame deflection is measured external to the housing by an LVDT. The sample is contained in the large concentric cylinder. There is no provision for maintenance of temperatures other than ambient at the present time. Shear rate is determined by shaft rotational velocity and cylinder geometry, neglecting edge effects.

Experimental Fluids

Eight liquid lubricants were employed in the high shear rate viscosity measurements. They are listed in Table 1 and described in the Appendix C. They include a polyphenyl ether (5P4E), a cycloaliphatic hydrocarbon (MCS 1218), dimethyl polysiloxanes (DC200-10^5, DC200-6 x 10^4, DC200-1.25 x 10^4), mineral oil - methacrylate blends (B3J and PL4520), and polybutenes (LF5195 and LF5196). They were selected because they had viscosities in a range which permitted high shear stresses to be developed in the instrument and had been previously studied in this laboratory.

Measurements

Viscosity, μ, is plotted as a function of shear rate, $\dot{\gamma}$, in Figure 2 for fluids DC200-100,000, DC200-12,500, 5P4E, MCS 1218, LF 5195, PL 4520 and B3J at 22C and 100 kPa (1 atm). 5P4E shows no effect of shear rate on viscosity to $\dot{\gamma} = 12{,}000\ s^{-1}$. The DC 200 fluids, MCS 1218 and LF 5195 display shear thinning while B3J undergoes a 50% increase in viscosity at about $10^3 s^{-1}$ above which it is known to shear thin.

As can be seen in Figure 3 there is little effect of pressure on the viscosity of LF 5195 in the shear rate range of 600 to 12,000 s^{-1} and for pressure to 400 kPa (4 atm). However, for DC200-60,000 silicone whose flow curve approaches constant stress with increasing shear rate at atmospheric pressure, a four-fold increase in pressure results in a $\simeq$65% increase in viscosity at $\dot{\gamma} = 6000\ s^{-1}$ and a reduction in the viscosity-shear rate slope. Below $\dot{\gamma} \cong 700\ s^{-1}$, its viscosity is unaffected by pressure.

Even more dramatic is the result for the polybutene LF 5196 in Figure 4. At $\dot{\gamma} = 1300\ s^{-1}$, an increase in pressure from 10 to 300 kPa increases the viscosity from 67 to 250 Pas, while the low shear rate viscosity is unaffected by pressure.

Conclusions

These preliminary measurements suggest the possible importance of low normal stress and cavitation or material fracture at high shear stresses. Because this type of stress field exists in elastohydrodynamic inlets and classical hydrodynamic configuration, such as high speed journal bearings, it should be further investigated, because it potentially represents a lubricant limitation to feeding bearings.

TRACTION REGIMES

The most commonly recognized modes of lubrication in concentrated contacts are boundary lubrication and elastohydrodynamic lubrication, and the mixed regime occurring upon transition between them. The transition between these two regimes must be understood because of its importance to wear, energy dissipation in the contact, and the life of the tribocontact. On the "elastohydrodynamic side" of this transition in concentrated contacts there is a tendency among many persons working in the field to believe that all non-conformal contacts operate in the elastohydrodynamic (or more precisely elastic-variable viscosity) regime. Over the past several years as a result of the works of several people [9,10] an appreciation has been gained for the importance of other regimes in the determination of film thickness behavior. It is now known that there are film thickness data in the literature attributed to the elastohydrodynamic regime which are in fact not from that regime. A similar situation may also exist in the case of concentrated contact traction data in the literature.

It is well known from film thickness analysis that as the speed parameter increases and the film thickness increases, the nature of the pressure distribution changes radically from the near Hertzian approximation to the more traditional rigid-isoviscous case of Martin for cylinders or Kapitza for spheres. The pressure distribution in the rigid-isoviscous case is more spread out and much lower in magnitude. These two pressure distributions will give quite different shear rheological behavior for the same lubricant. In the case of the concentrated Hertzian type distribution the lubricant is expected to behave as an elastic-plastic amorphous solid which has a limiting shear stress as a linear function of temperature and pressure controlling the traction. For the lower pressure, thicker film case, the lubricant will behave as a liquid with a viscosity which has an exponential variation with temperature and pressure to determine traction [11].

It will be shown, in the elastohydrodynamic regime when the sliding component of the contact kinematics is large enough to avoid the elastic lubricant behavior associated with nearly pure rolling, that the traction is a linear function of temperature. On the low film thickness side of that regime the traction increases as the film thickness decreases as expected from lambda ratio considerations as the contact enters the mixed film regime. On the thick film side of the elastohydrodynamic regime the traction decreases as film thickness increases due to the change in rheological behavior to lower pressure viscous behavior of the lubricant.

Experimental Fluids

Seven liquid lubricants were used in this program. They are listed in Table 2. These fluids have all been used in previous reports [1,2,3,4,13]. Brief descriptions of the fluids are given in Appendix C.

Experimental Method

The concentrated contact simulator was discussed previously [2,12]. Traction was measured for the seven fluids while varying the film thickness and slide-to-roll ratio. Film thickness was varied by varying both the rolling velocity and the bulk temperature of the system. Most of the data was taken at a Hertz pressure of 1.08 GPa but some was at 1.24 GPa. The bulk temperature was varied from 20 to 90C. The composite surface roughness for most of the data was 0.05 μm while some was for 0.12 μm rms. The sapphire was essentially smooth and all the composite roughness was associated with the roller. The surface roughness was determined by using a sampling length of five times the contact diameter in accordance with the findings of Nagaraj and Winer [14].

The traction coefficient at $\Sigma = 0.15$ was chosen to compare the traction behavior of the fluids. The viscosity and pressure viscosity coefficient of the fluids have been measured in our laboratory (coefficients are listed in Table 3). None of the fluids contained high polymers except Santotrac 50 and therefore the film thickness was calculated with confidence [15] using the Hamrock and Dowson equation [15]. For all fluids, except the diester, the limiting shear stress has been measured in this laboratory and reported elsewhere [1]. The film thicknesses reported are all calculated values.

Presentation and Discussion of Results

Figure 5 shows the variation of traction coefficient as a function of temperature for six fluids. It also has plotted on the right hand side the ratio of the measured limiting shear stress divided by the average Hertz pressure ($0.67\ p_H$) at the indicated temperatures. If the limiting shear stress is the property determining the traction, agreement between the measured traction and the measured limiting shear stress ratio should be good. This seems to be the case for all but the LVI-260 and the Vitrea 79. These are both fairly viscous fluids and the film thickness in the traction experiment is large at the temperature at which limiting stress was measured. Figures 6a and 6b show similar data for the diester but with both temperature and rolling velocity varying. For high speed and/or low temperature, where the thickest films would be expected, the traction appears to be independent of speed and a linear function

of temperature as expected from the limiting shear stress model. At low speed where the EHD films calculated are of the same magnitude as the composite surface roughness, the traction increases as temperature increases indicating mixed film behavior with increased asperity friction.

For each data point indicated in Figure 6 the film thickness, and therefore the lambda ratio, can be calculated. From that calculation we find that most of the data for the highest two velocities have lambda ratios greater than one. If we assume that for those two speeds the traction is the result of the limiting shear stress of the lubricant and that the limiting shear stress is a function of temperature, we can calculate a reduced traction for each data point. This is equal to the traction which was measured, divided by the traction expected at that temperature from the limiting shear stress. The plot of this reduced traction against lambda ratio is shown in Figure 7. Not surprisingly the reduced traction is quite constant for lambda ratios greater than one where the traction is the result of shearing the lubricant film and increases substantially as the lambda ratio is reduced below one where asperity friction begins in the mixed film regime. As the lambda ratio is reduced the load is being shifted from the EHD fluid film on to the asperities.

Another approach to examining the data is shown in Figure 8 for the other six lubricants where traction coefficient is plotted against lambda ratio. In five of the six cases there is clearly a straight line region for lambda ratio (somewhat greater than one to about 15). Note that temperature increases to the left (thinner films). These data again show the increase of traction as lambda approaches one (e.g., N1/R620-15) and also show the decrease of traction for the larger values of lambda (e.g., about 20). The regime in between might be considered the classical EHD regime where the traction is the result of the limiting shear stress which is a linear function of temperature. If we take the view that the traction in this range of lambda ratio should be a function of temperature through the limiting shear stress as was donewith the diester, we can again calculate a reduced traction coefficient. This reduced traction coefficient is the ratio of the measured traction coefficient to what would be expected if the traction were determined by the limiting shear stress at the same temperature. Results from Figure 8 along with those for the diester from Figure 7 and some additional data at different surface roughness are plotted in Figure 9.

The pattern of behavior becomes quite clear in Figure 9. In a range of lambda ratio from 1 or 1.5 to 15 or 20 the reduced lambda ratio is one implying that the traction is controlled by the limiting shear stress which is a linear function of temperature. For lambda

less than about one the EHD film is so thin it begins to share the load with the asperities resulting in the increased traction associated with mixed lubrication. At lambda ratios of more than twenty the film thickness is large and the surface deformation is approaching the undeformed surface resulting in a spread out and reduced pressure distribution. This reduced pressure distribution moves the lubricant behavior toward the viscous regime of behavior and therefore lower traction [11].

If we examine the high lambda ratio transition in light of information in the literature on EHD film thickness regimes and pressure distributions, we can support the above interpretation of the behavior. For example, Hamrock and Dowson [16] show that for a speed parameter $U = 0.5 \times 10^{-10}$ the pressure profile has sifted from a recognizable Hertz profile to the sharply pointed form similar to Martin's for rigid solids. Hamrock and Dowson's speed parameter U is shown double scaled with the lambda ratio in Figure 9. To the extent the comparison can be made with line contact behavior, Dowson and Higginson [11] show that in the range of speed parameter of about 10^{-9} the pressure profile flattens out to a broad low profile within one half order of magnitude.

If we compare the traction behavior with film thickness regime charts, we can use either the Hamrock and Dowson regime plots [9] or those of Moes and Bosma [10]. In the case of Hamrock and Dowson's, all the data shown in Figure 9 is along the border between the viscous-elastic and the viscous-rigid regimes but well away from the isoviscous-rigid regime. The highest lambda ratio point on Figure 9 has a dimensionless viscosity parameter value about ten times the value of that parameter on the boundary between the isoviscous-rigid and the elastic-viscous regimes. While the value of the elasticity parameter is about the same as that of the boundary between the rigid-isoviscous and the elastic isoviscous regimes. The bend is in the farthest region of their regime chart. That is, the only portion of Figure 7 that falls within the regime chart they have presented is that above lambda ratio of twenty. All the other data of Figure 9 would be further into the more severe elastohydrodynamic region of their chart.

If we compare the range of data with the Moes and Bosma dimensionless groups, they show the transition from rigid-isoviscous to elastic-viscous occurring at a value of 8 to 10 for one dimensionless group (M) depending somewhat on the second dimensionless group (L). The value of M = 10 of Figure 9 appears at the end of the curve which is interpreted as the transition in traction behavior from limiting shear stress behavior to viscous behavior. M increases to the left in Figure 9 which is in the direction of the EHD regime on their chart. The recent EHD point contact solutions of Evans and Snidle [18] appear to agree with the transition in terms of the Moes and Bosma variables.

Conclusions

The traction behavior of concentrated contacts is complex and can be divided into several regimes depending on the lubricant, the solid surface, and operating conditions. For lambda ratios of about two to twenty the lubricant behavior can be elastic-viscous-plastic for slide-roll ratios near zero [11]. While for slide-roll ratios greater than about 0.03 the traction behavior is plastic controlled by the limiting shear stress which is a linear function of temperature and pressure. The limiting shear stress and therefore traction increases with increasing pressure and decreasing temperature. For lambda ratios less than about two the contact moves into the mixed film regime with load sharing shifting away from the EHD film to the asperities as lambda ratio decreases resulting in increased traction and increased local surface temperatures. As the lambda ratio and the speed parameter (U) increase, the traction decreases as a result of the pressure in the film decreasing and the lubricant behavior becoming viscous in nature. At this thick film condition, the traction transition behavior is controlled by the speed parameter (U) while for the thin film case the traction transition is controlled by the lambda ratio.

ADDITIONAL TRACTION MEASUREMENTS

Traction measurements on a number of additional lubricants were made to determine the traction as a function of material, slide-to-roll ratio, rolling speed, temperature and side-slip angle.

The side-slip angle is defined as the angle between a line through the center of contact area passing through and perpendicular to the axis of rotation of the disk, and the axis of rotation of the roller. A zero side-slip angle implies that the axis of rotation of the roller passes through the axis of rotation of the disk.

Figures 10-15 contain results of traction measurements on various materials for contact aspect ratio of 1, Hertz Pressure 1.0 GPa and temperature and velocity shown. The liquid lubricants Santotrac 50 and diester have been described in previous reports [1,2,3,19]. The Santotrac 50 data in Figures 10a and b show the effect of side-slip angle, θ, on reducing the slope of the traction versus slide-roll ratio curve. The Conoco Traction Fluid (sample 8915L) was supplied by NASA-Lewis. Figures 11a-11g illustrate the effects of speed, temperature, and side-slip angle on the traction characteristics of the Conoco sample.

The traction characteristics of a MIL-L7808 fluid (diester) are depicted in Figure 12.

A polyethelene grease was smeared on the steel disc to produce Figure 13. Shown is the data for the first traverse of the grease-covered disc. Subsequent traverses produced higher traction coefficients at radial positions of the disc where lubricant had been "plowed" away.

Figures 14 and 15 represent dry discs burnished with block Teflon and MoS_2 powder respectively.

In addition, the traction behavior of the two base oils R620-15 and R620-16, and two polymer-oil blends, R620-15 + PL4521 and PL4523, (used in the next section) was measured for an aspect ratio of 2.5, peak Hertz pressure of p_H = 1.0 GPa, and temperature of T = 26C. As is expected from limiting shear stress measurements [2] the four percent addition of the methacrylate polymer reduces the traction coefficient of the R620-15 (Figure 16). At 1 m/s for R620-15, the speed parameter $U = 1.2 \times 10^{-10}$ indicating that the fall-off of traction with speed is due to pressure reduction as the hydrodynamic traction regime is entered as discussed in the previous section.

FILM THICKNESS MEASUREMENTS

Polymers in lubricants are known to increase the low shear viscosity of the solvent (base oil) but the film thickness generated in an elastohydrodynamic contact with a polymer blend is not as large as expected from the standard EHD film thickness calculation using the low shear viscosity. A conservative engineering guideline in the case of polymer blended materials is to assume that the base oil viscosity controls the film thickness. However, this may be unnecessarily conservative. The measurements reported here were to determine the effective viscosity of a polymer blend based on the EHD film thickness generated by the blend.

Optical interferometry was used to measure lubricant film thickness during the operation of the simulator. A microscope with a through the lens light source was focussed on the contact. A narrow band pass filter (Wrattan 72B) with a dominant wavelength (λ = 605 nm) was used between the tungsten lamp and microscope. An aspect ratio of k = 2.5 was used, resulting in a Hertz pressure of p_H = 0.80 GPa from a load, w = 25N. Nearly pure rolling (Σ = 0) was obtained by removing the drive belt from the roller and allowing the roller to be driven by the disk. An uncoated sapphire disc was utilized.

With this interference technique, changes in thickness of the film are viewed as alternate light and dark fringes appearing in the contact. The film thickness where a bright fringe occurs is

$$h_+ = \frac{\lambda}{2\zeta}\left(n + \frac{\Delta\phi}{2\pi}\right), \quad n = 0,1,2,\ldots$$

and where a dark fringe occurs is

$$h_- = \frac{\lambda}{2\zeta}\left(n + \frac{\Delta\phi}{2\pi} + \frac{1}{2}\right), \quad n = 0,1,2,\ldots$$

Where $\Delta\phi$ is the phase change due to roughness of the roller surface and n is the fringe order. The fluid refractive index, ζ, was taken to be 1.5 in all cases. This leaves $\Delta\phi$ to be calibrated for the particular system.

For four fluid samples (two base oils and two polymer blends, described in Appendix C), rolling speed was increased until a light or dark fringe was observed in the center of the contact. The speed and fringe order was noted.

The system calibration was done with a convenient motor oil (S-6) and is shown in Figure 17. A plot of fringe order (n - 1/2 for dark fringes) versus $\bar{V}^{0.67}$ yields a straight line whose intercept is

$$\frac{2\zeta h}{\lambda} - \frac{\Delta\phi}{2\pi} = -0.42 \ .$$

Since at $\bar{V} = 0$, $h = 0$,

$$\frac{\Delta\phi}{2\pi} = 0.42 \ .$$

Film thicknesses were observed at 26C, 50C, and 75C and are plotted for all samples in Figures 18-21. The open symbols represent bright fringe values and the solid symbols represent dark fringe values. Also plotted are film thickness predictions from the relation [20],

$$h_c = 2.69 \ R_x U^{0.67} G^{0.53} W^{-0.067} (1 - 0.61 \ e^{-0.73k})$$

for central film thickness. Where

$$W = \frac{w}{ER_x^2}$$

$$U = \frac{\mu_o \bar{V}}{ER_x}$$

$$G = \alpha E$$

$$\frac{1}{E} = \frac{1}{2}\left(\frac{1-\nu_1^2}{E_1} + \frac{1-\nu_2^2}{E_2}\right)$$

E_1, E_2, ν_1 and ν_2 are moduli of elasticity and Poisson's ratio for the disk and roller and R_x is the roller radius in the direction of motion, and k is the ellipticity ratio of the contact area (contact semi-axis perpendicular to the direction of motion divided by the contact semi-axis in the direction of motion). The pressure-viscosity data measured and presented in Table 3 were used in these calculations.

For oils R620-15 and R620-16 which are known to contain no polymer V.I. improver the agreement between measured and predicted film thickness is satisfactory. For other materials the viscosity data predicts higher values than those measured. In particular, the

measured film thickness for R620-15 + PL4523 (2×10^6 M.W. PAMA) is one-third of the predicted value. For the experimental blends (R620-15 + PL4521 and R620-15 + PL4523) the film thickness predicted from base oil properties is also plotted and the measured values lie between each pair of predicted curves.

From these plots it could be suggested that the rheological properties that determine the film thickness (i.e., μ_o and α in the high shear inlet region of the concentrated contact) for the polymer-oil blend are reduced from the values measured for the blend at low shear stress to those more representative of the base oil. Since the pressure-viscosity coefficient of the base oil is nearly the same as the blend it can be assumed that α does not change and the viscosity is responsible for the reduced film thickness. Therefore an effective viscosity, μ_{EFF}, can be calculated from the film thickness data and the film thickness relations. These are tabulated in Table 4 and plotted against low shear rate viscosity for the base oil with and without polymer in Figure 22.

Conclusions

The use of base oil viscosity to predict EHD film thickness of polymer-oil blends is too conservative. Effective inlet viscosity is intermediate between blend and base oil low shear rate viscosity.

Figure 22 suggests the following relationship

$$\log \mu_{eff} = \log \mu_{o_{base}} + K(\log \mu_{o_{blend}} - \mu_{o_{base}})$$

where

$$K = \frac{\log \mu_{eff} - \log \mu_{o_{base}}}{\log \mu_{o_{blend}} - \log \mu_{o_{base}}}$$

Then

$$\mu_{eff} = \mu_{o_{base}} \left(\frac{\mu_{o_{blend}}}{\mu_{o_{base}}} \right)^K .$$

The parameter K can be thought of as the EHD film forming enhancement efficiency of the polymer in the given base oil. The addition of the polymer to the base oil is expected to increase the EHD film thickness in relation to its influence on increasing the viscosity of the blend over that of the base oil. However, the increase in EHD film thickness is less that expected from classical EHD film thickness calculations using the low shear viscosity. The EHD film forming enhancement parameter K ($0 \leqslant K \leqslant 1.0$) indicates the fraction of film thickness increase expected that actually occurs.

Values of K are tabulated in Table 5. The average K for 4% by weight of polyalkylmethacrylate is 0.29 and is somewhat lower (0.26) for the high molecular weight material than for the lower molecular weight material (0.32). K can be a convenient factor for describing the film thickness building capability of a polymer relative to its viscosity building capability.

REFERENCES

1. Bair, S. and W. O. Winer. "Surface Temperatures and Glassy State Investigations in Tribology - Part III", NASA Contractor Report 3272 (April 1980).

2. Bair, S. and W. O. Winer. "Surface Temperatures and Glassy State Investigations in Tribology - Part IV", NASA Contractor Report 3368 (January 1981).

3. Bair, S. and W. O. Winer. "Surface Temperatures and Glassy State Investigations in Tribology - Part II", NASA Contractor Report 3162 (July 1979).

4. Winer, W. O., and Sanborn, D. M., "Surface Temperatures and Glassy State Investigations in Tribology", NASA CR3031 (Part I) (June 1978).

5. Wyman, Elyash and Frayer. "Comparison of Some Mechanical and Flow Properties of Linear and Tetra-chain Branched 'Monodisperse' Polystyrenes", *Journal of Polymer Science 3*, Part A (1965) 681-696.

6. Stratton, Robert. "Non-Newtonian Flow in Polymer Systems with no Entanglement Coupling", *Journal of Polymer Science 5*, No. 3 (May-June 1972) 304-310.

7. Yoshio Ito and Shernsuke Shishido. "Critical Molecular Weight for Onset of Non-Newtonian Flow and Upper Newtonian Viscosity of Polydimethylsiloxane", *Journal of Polymer Science: Polymer Physics Edition, 10*, (1972) 2239-2248.

8. Stratton, Robert A. "The Dependence on non-Newtonian Viscosity on Molecular Weight for 'Monodisperse' Polystyrene", *Journal of Colloid and Interface Science 22* (1966) 517-530.

9. Hamrock, B. J., and D. Dowson. "Minimum Film Thickness in Elliptical Contacts for Different Regimes of Fluid-film Lubrication", NASA Technical Paper 1342 (October 1978).

10. Moes, H., and R. Bosma. "Film Thickness and Traction in EHL at Point Contact", *Proceedings of Elastohydrodynamic Symposium* (1972) Institute of Mechanical Engineers, London, Paper C38/72, 149-152.

11. Bair, S., and W. O. Winer. "A Rheological Model of Elastohydrodynamic Contacts Based on Primary Laboratory Data', *Trans. ASME, Journal of Lubrication Technology 101, 3* (July 1979) 258-265.

12. Bair, S., and W. O. Winer. "Friction/Traction Measurement with Continuously Variable Slide-Roll Ratio and Side Slip at Various Lambda-Ratios", *Proceedings of the 1980 Leeds-Lyon Conference* (1980).

13. Johnson, K. L., and J. L. Tevaarwerk. "Shear Behavior of Elastohydrodynamic Oil Films", *Proc. Roy. Soc. of London,* 365A (1977) 215-236.

14. Nagaraj, H. S., D. M. Sanborn, and W. O. Winer. "The Effect of Surface Roughness of Surface Temperature Fluctuations in EHD Contacts", *Proceedings of 4th Leeds-Lyon Symposium on Tribology,* D. Dowson, C. M. Taylor, M. Godet (editors) Mechanical Engineering Publications Ltd. (1978) 141-147.

15. Koye, K. A., and W. O. Winer, "An Experimental Evaluation of the Hamrock and Dowson Minimum Film Thickness Equation for Fully Flooded EHD Point Contacts", *Trans. ASME, Journal of Lubrication Technology, 103,* No. 2 (April 1981).

16. Hamrock, B. J., and D. Dowson. "Isothermal Elastohydrodynamic Lubrication of Point Contacts: Part 3 - Fully Flooded Results", *Trans. ASME, Journal of Lubrication Technology, 99* (1977) 264.

17. Dowson, D., and G. R. Higginson. *Elast-Hydrodynamic Lubrication,* Pergamon Press, New York (1966).

18. Evans, H. P., and R. W. Snidle. "The Isothermal Elastohydrodynamic Lubrication of Spheres", *Trans. ASME, Journal of Lubrication Technology, 103,* No. 2 (April 1981).

19. Winer, W. O., and D. M. Sanborn, "Lubricant Rheology Applied to EHD Lubrication", NASA Contractor Report 2837 (May 1977).

20. Hamrock, B. J., and Dowson, D. "Isothermal Elastohydrodynamic Lubrication of Point Contacts: Part 3 - Fully Flooded Results", *Trans. ASME, Journal of Lubrication Technology, 99* (1977) 264.

APPENDIX A

SHEAR STRENGTH MEASUREMENTS OF ULTRA HIGH MOLECULAR WEIGHT POLYETHELENE AT HIGH PRESSURE

(Material Supplied by NASA-Lewis)

GEORGIA INSTITUTE OF TECHNOLOGY
ATLANTA, GEORGIA 30332

SCHOOL OF
MECHANICAL ENGINEERING

30 January 1981

Dr. William R. Jones
NASA-Lewis Research Center
21000 Brookpark Road (MS23-2)
Cleveland, Ohio 44135

Dear Bill:

Sorry for the delay in providing shear strength data on the ultra-high Molecular weight polyethylene. The instrumentation for the shear strength apparatus is used in other experiments and just recently became available.

The stress strain curves included were traced directly from the recorder plot. Two polyethylene specimens were used to generate the four curves for polyethylene and one poly-vinyl chloride specimen was sheared to provide a calibration check of the equipment. The results are summarized in the graph. The tailed data points for PVC are the most recent.

In addition, a simple measurement of shear strength at atmospheric pressure was performed by measuring the force to shear a center segment from a 0.077 inch diameter pin. The results are as follows for the polymers we have investigated:

Material	S_s/MPa
PVC	57
TFE	20
NYLON	63
PAMA	68
UHMWPE	40

Sincerely,

Scott Bair
Research Engineer

jmv
attachment

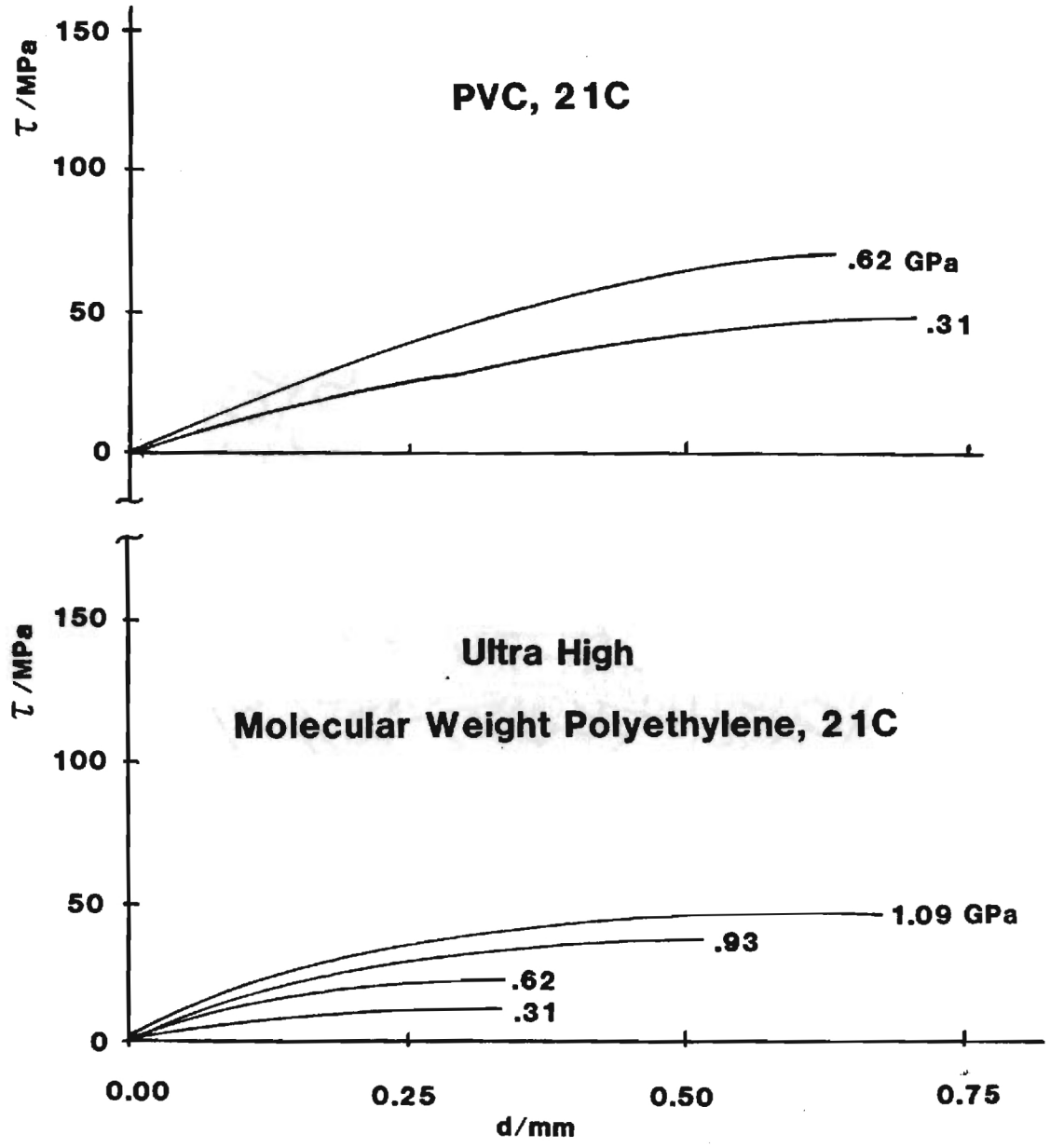
PVC, 21C
τ /MPa
150
100
50
0
.62 GPa
.31
Ultra High
Molecular Weight Polyethylene, 21C
τ /MPa
150
100
50
0
1.09 GPa
.93
.62
.31
0.00
0.25
0.50
0.75
d/mm

APPENDIX A

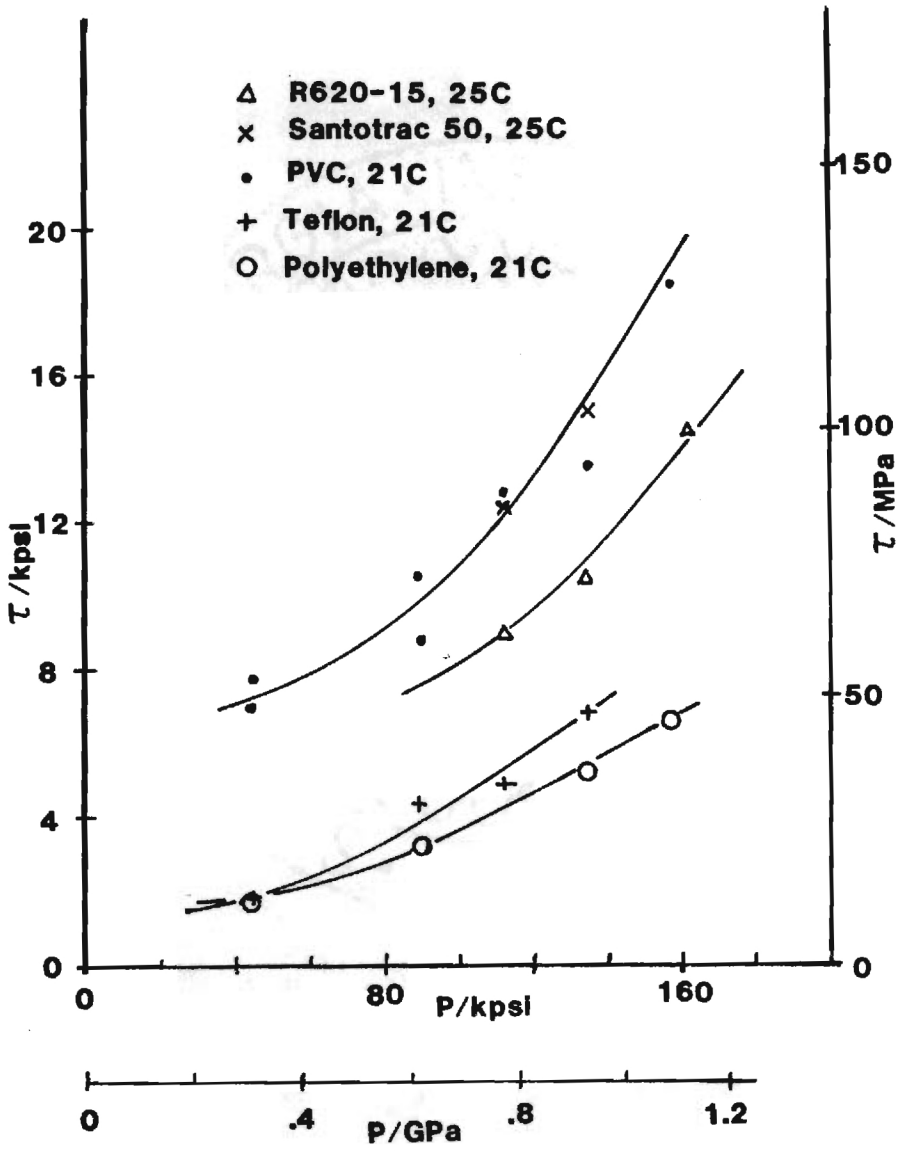
Δ R620-15, 25C
× Santotrac 50, 25C
• PVC, 21C
+ Teflon, 21C
○ Polyethylene, 21C
20
16
12
8
4
0
τ/kpsi
150
100
50
0
τ/MPa
0
80
160
P/kpsi
0
.4
.8
1.2
P/GPa

APPENDIX B

PRESSURE-VISCOSITY MEASUREMENTS OF BRAYCO MICRONIC 815Z

APPENDIX B

PRESSURE-VISCOSITY MEASUREMENTS OF BRAYCO MICRONIC 815Z

GEORGIA INSTITUTE OF TECHNOLOGY
ATLANTA, GEORGIA 30332

SCHOOL OF
MECHANICAL ENGINEERING

13 August 1981

Mr. Tim Clark
Goddard Space Flight Center
NASA
Greenbelt, Maryland 20770

Dear Tim:

The check on the pressure-viscosity characteristics of Brayco Micronic 815Z received August 6 is complete and the results follow:

FLUID: MICRONIC 815Z - Batch GLG9

SOURCE: Goddard Space Flight Center

T/C	P/KPSI	/GPa	μ/cp(mPas)
38.3	ATM	ATM	232
38.2	5	0.034	521
38.0	10	0.069	873
37.6	15	0.103	1691
37.6	20	0.138	3336
99.2	ATM	ATM	56.6
98.8	5	0.034	131.3
98.8	10	0.069	241
98.5	20	0.138	582
98.5	40	0.276	2040
98.3	60	0.413	7370

COMMENTS:

Sample was contaminated as received. Appeared milky and was separated by density at top surface. The odor of ethanol was apparent. Heating produced low temperature boiling and a flame above test tube containing the sample after which the liquid was clear and colorless. The test was performed on a boiled sample.

PRESSURE COEFFICIENTS:	38C	99C
a_{OT}/GPa^{-1}	18.9	24.65
a_T^*/GPa^{-1}	18.9	15.95

Also enclosed is a graph comparing this sample to the one previously tested (batch BLD4). There is the possibility that some ethanol remained in the new sample during the test accounting for discrepancies in the data.

Sincerely yours,

Scott Bair
Research Engineer

jmv

cc: Vern Wedeven
Bill Jones

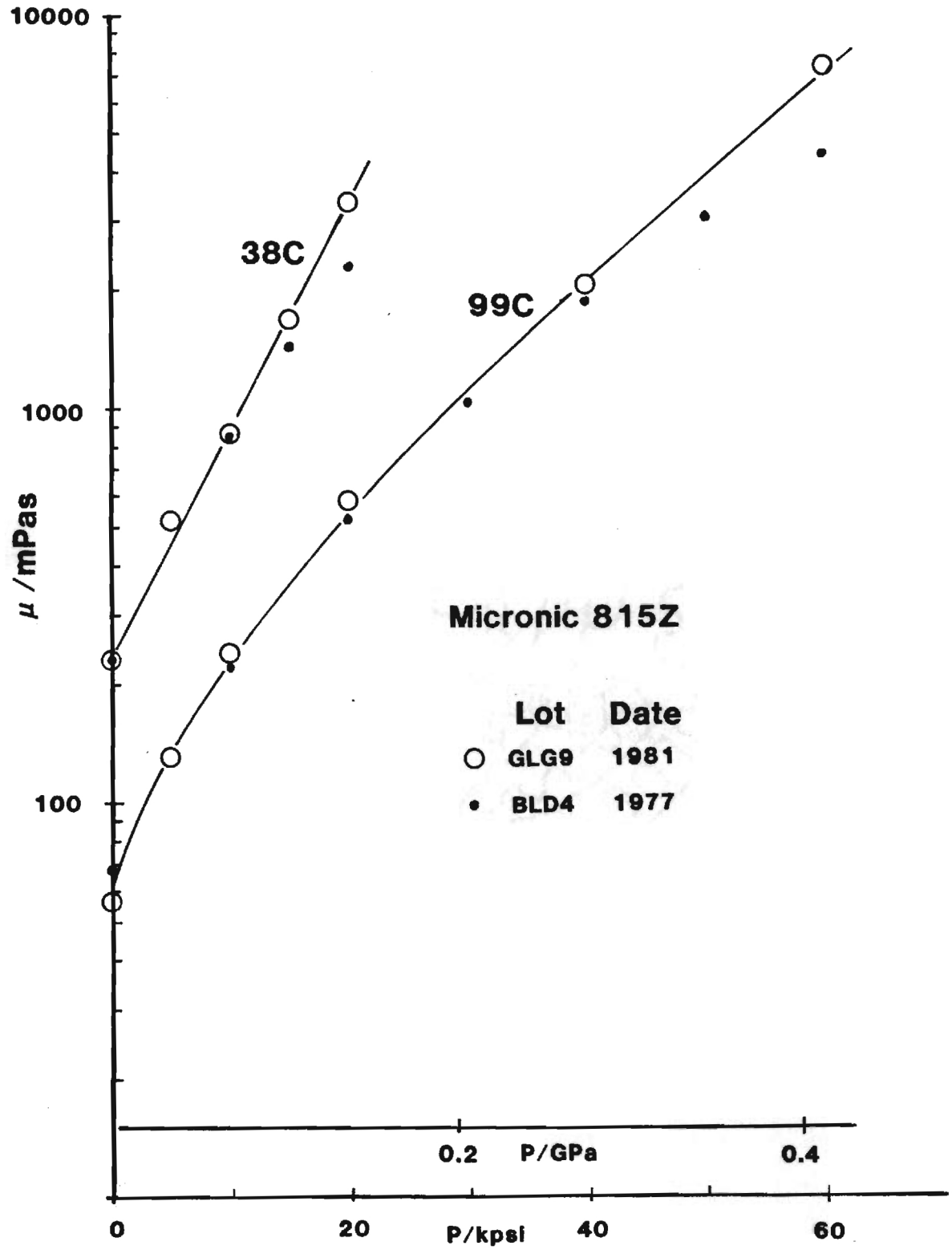
10000
1000
100
μ /mPas
38C
99C
Micronic 815Z
Lot Date
GLG9 1981
BLD4 1977
0.2 P/GPa 0.4
0
20
P/kpsi
40
60

APPENDIX C

FLUID DESCRIPTION

Symbol:	5P4E	
Type:	Five-ring Polyphenyl Ether	
Source:	Monsanto Company	
Properties:	Viscosity at 37,8C, m^2/s	363×10^{-6}
	Viscosity at 98.9C, m^2/s	13.1×10^{-6}
	Density at 22.2C, kg/m^3	1205
	Density at 37.8C, kg/m^3	1190
	Flash Point, C	288
	Pour Point, C	4.4

Symbol:	MCS-1218	
Source:	Monsanto Company	
Type:	Cycloaliphatic Hydrocarbon	
Properties:	It is a combination of two components each having a molecular weight less than 1000.	
	Viscosity at 37.8C, m^2/s	1418×10^{-6}
	Viscosity at 98.9C, m^2/s	18.37×10^{-6}
	Density at 23.9C, kg/m^3	940

Symbol: LF5195 and LF5196

Source: American Oil Company

Type: Polybutene

Properties:

	LF5195	LF5196
Viscosity at 37.8C, m^2/s	8.067×10^{-3}	---
Viscosity at 98.9C, m^2/s	219×10^{-6}	3.325×10^{-3}
Density at 25C, kg/m^3	889	916
Molecular Weight (Number Average)	902	2191

Symbol: B3J

Source: Blend of Sun Oil Company base oil (R620-12) and Polymer of Rohm and Haas Company

Type: Paraffinic base oil with PL4523 Polymethacrylate

Properties:

Viscosity at 37.8C, m^2/s	33.3×10^{-6}
Viscosity at 98.9C, m^2/s	5.336×10^{-6}
Viscosity Index (ASTM D-2270)	102
Flash Point, C	210
Pour Point, C	-15
Density at 20C, kg/m^3	860
Molecular Weight	401

Symbol: DC200-100,000/ -60,000/ -12,500

Source: Dow Corning Company

Type: Dimethyl Polysiloxane

Properties:	100,000	60,000	12,500
Viscosity at 25C, m^2/s	0.1	0.06	0.0125

Symbol: Krytox 143-AB (Lot 10)

Type: Perfluorinated polyether

Source: DuPont Company

Properties:	
Viscosity at 37.8C, m^2/s	96.6×10^{-6}
Viscosity at 98.9C, m^2/s	11.5×10^{-6}
Density at 24C, kg/m^3	1890
Density at 98.9C, kg/m^3	1760
V.I. (ASTM D-2270)	116
Pour point, C	-40
Flammability	does not burn

Symbol:	Diester	
Source:	Rohm and Haas Company	
Type:	Diester-Plexol 201 bis-2-ethyl hexyl sebecate (PL 5159)	
Properties:	Viscosity at -53.9C m^2/s	7988×10^{-6}
	Viscosity at 37.8C m^2/s	12.75×10^{-6}
	Viscosity at 98.9C m^2/s	3.32×10^{-6}
	Cloud Point (ASTM D-2500)	below -54C

Symbol:	R620-16	
Source:	Sun Oil Company	
Type:	Naphthenic Base Oil	
Properties:	Viscosity at 37.8C m^2/s	114.2×10^{-6}
	Viscosity at 98.9C m^2/s	8.076×10^{-6}
	Viscosity Index (D-2270)	< 0
	Density at 20C, kg/m^3	930.3
	Average Molecular Weight	357
	Refractive Index	1.5173
	Pour Point C	-23

Symbol:	R620-15 (N1)	
Source:	Sun Oil Company	
Type:	Naphthenic Base Oil	
Properties:	Viscosity at 37.8C, m^2/s	24.1×10^{-6}
	Viscosity at 98.9C, m^2/s	3.73×10^{-6}
	Viscosity Index (ASTM D-2270)	-13
	Flash Point, C	157
	Pour Point, C	-43
	Density at 20C, kg/m^3	915.7
	Average Molecular Weight	305

Symbol:	Santotrac 50	
Source:	Monsanto Company	
Type:	Synthetic Cycloaliphatic Hydrocarbon Traction Fluid	
Properties:	Viscosity at 37.8C, m^2/s	34×10^{-6}
	Viscosity at 98.9C, m^2/s	5.6×10^{-6}
	Pour Point, C	-37
	Density at 37.8C, kg/m^3	889
	Flash Point, C	163
	Fire Point, C	174
	Specific Heat at 37.8C, J/Kg·K	2332

Additive package includes: Antiwear (zinc dialkyl dithiophosphate), Oxidation inhibitor, Antifoam, VI Improver (Polymethacrylate).

Symbol: LVI 260

Source: Shell Oil Company (via K. L. Johnson)

Type: LVI High Viscosity Oil

47% saturates and 53% aromatics

Properties: (From K. L. Johnson)

Viscosity at 37.8C, m^2/sec	338×10^{-6}
Viscosity at 98.9C, m^2/sec	232×10^{-6}
Density at 15.5C, kg/m^3	929
Specific gravity, 60/60F	0.929
Viscosity pressure coefficient at 37.8C, m^2/N	34.2×10^{-9}

Symbol: Shell Vitrea 79

Source: Shell Oil Company (Via K. L. Johnson)

Type: HVI high viscosity oil

Predominantly naphthenic and paraffinic

Properties: (From K. L. Johnson)

Viscosity at 37.8C, m^2/sec	581×10^{-6}
Viscosity at 98.9C, m^2/sec	75×10^{-6}
Density at 15.5C, kg/m^3	886
Specific gravity, 60.60F	0.886
Viscosity pressure coefficient at 37.8C, m^2/N	25×10^{-9}

Symbol:	PL4520, PL4521, PL4523		
Source:	Rohm and Haas Company		
Type:	Polyalkylmethacrylate [Polymer additive used in solution in R620-15, 4.0% polymer by weight] The chemical composition of each is the same. They differ only in molecular weight and are supplied in a carrier oil similar to R620-15.		
Properties:	PL4520	PL4521	PL4523
Polymer Concentration by Weight:	42.6%	36.1%	19.0%
Viscosity Average Molecular Weight:	355×10^3	560×10^3	2×10^6
Viscosity, mm^2/s at 98.9C	820		

Symbol:	S-6
Source:	Quaker State
Type:	Commercial SAE 30 Motor Oil API-SC

TABLES

Table 1. High Shear Rate Viscometry

Samples	
5P4E	Five-ring polyphenyl ether
MCS 1218	Cycloaliphatic hydrocarbon
LF5195	Polybutene
LF5196	Polybutene
PL4520	Polyalkylmethacrylate
B3J	Paraffinic plus polyalkylmethacrylate
DC200-100,000	Dimethylpolysiloxane
DC200- 60,000	Dimethylpolysiloxane
DC200- 12,500	Dimethylpolysiloxane

Table 2. Traction Regime Fluids

Samples	
Diester	Bis-2-ethyl hexyl sebecate
N1	Naphthenic Mineral Oil/R620-15
5P4E	Five-ring polyphenyl ether
Krytox	Perfluorinated polyether
Santotrac 50	Synthetic Cycloaliphatic hydrocarbon
LVI 260	Mineral Oil
Vitrea 79	Mineral Oil

Table 3. Pressure-Viscosity Coefficients

Fluid	TEMP/C	α_{OT}	α_T^*
R620-15	26	27.4	27.4
	40	21.9	21.9
	99	15.4	14.8
	149	10.7	11.0
	227	12.0	8.85
R620-16	26	35.6	35.8
	99	19.8	19.8
	227	10.8	10.6
R620-15 + PL4523	26	25.5	25.7
	99	17.1	15.0
	227	16.8	10.3
R620-15 + PL4521	26	24.2	24.9
	99	15.0	15.3
	227	13.8	9.8
5P4E	40	40.6	41.2
	60	27.6	29.3
	80	20.0	20.1
	227	6.8	6.8
LVI 260	30	31.9	34.8
VITREA 79	30	22.6	22.6
	40	22.6	22.6

$$\alpha_{OT} \equiv \left.\frac{d\ell n\,\mu}{dp}\right|_{T,p\,=\,0} \qquad \alpha_T^* \equiv \left[\int_o^{p\to\infty} \frac{\mu(T,p=0)}{\mu(T,p)}\,dp\right]^{-1}\Bigg|_T$$

Table 4. Effective Inlet Viscosity from Film Thickness Measurements Compared to Low Shear Viscosity in mPas

Fluid	25C (26C)		50C		75C	
	μ_o Low Shear Viscosity	μ_{EFF} Effective Viscosity[1]	μ_o Low Shear Viscosity	μ_{EFF} Effective Viscosity[1]	μ_o Low Shear Viscosity	μ_{EFF} Effective Viscosity[2]
R620-16	270	229	55	47.5	18	15.4
R620-15	37	43.0	12	11.0	5.25	--
R620-15 + PL4521	116	54.7	45	16.9	21	8.67
R620-15 + PL4523	370	66.4	140	24.5	61	9.52

[1]At rolling speed of 1 m/s

[2]At central film thickness of 0.18 μm

Table 5. Tabulation of the Factor, K, for Polymer Thickened Oils

K

TEMPERATURE	26C	50C	75C	AVERAGE
FLUID				
R620-15 + PL4521	0.34	0.26	0.36	0.32
R620-15 + PL4423	0.25	0.29	0.24	0.26

ILLUSTRATIONS

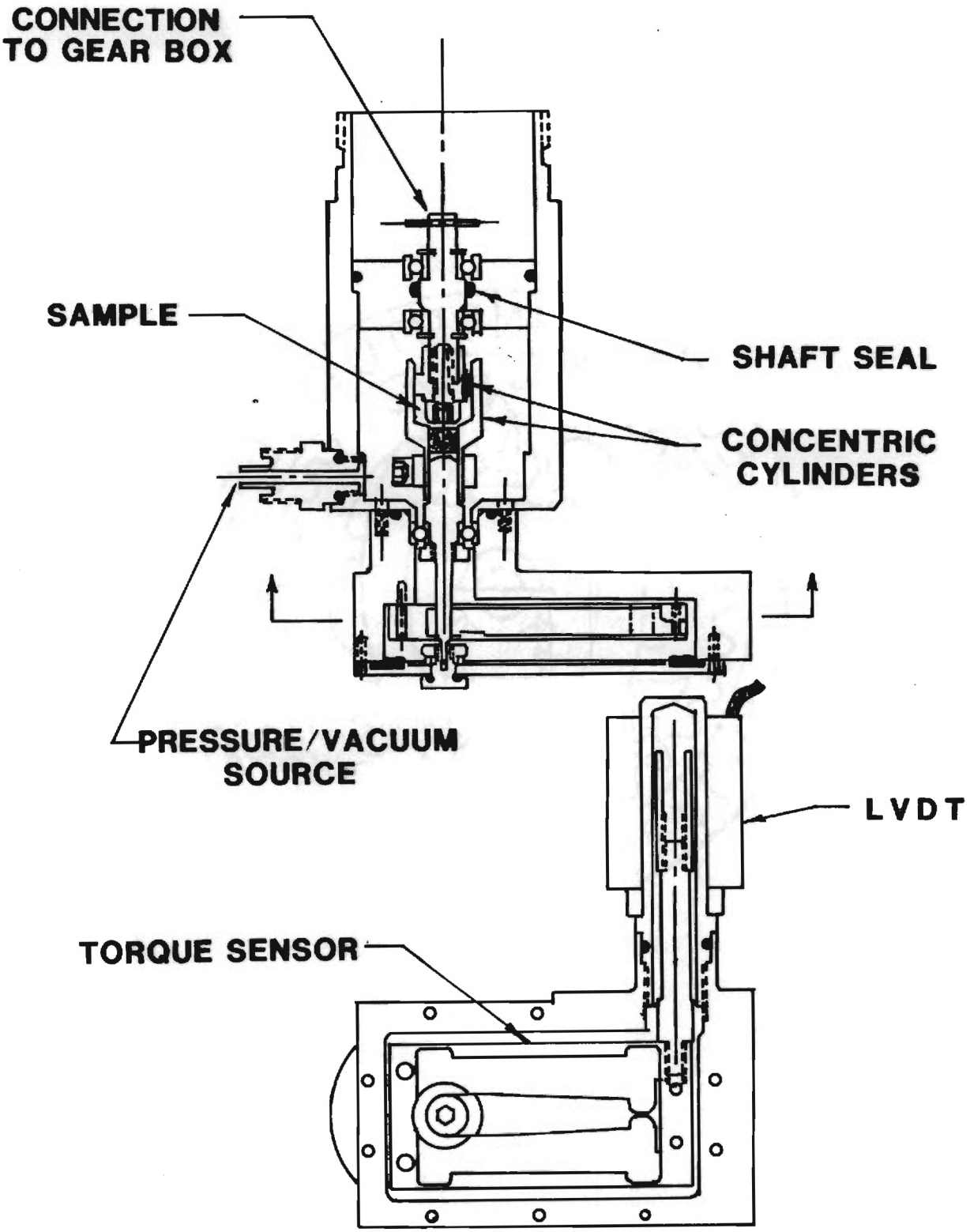

Figure 1. Rotary Viscometer ($10^1 < \dot{\gamma} < 10^4 s^{-1}$, $5 \times 10^3 < P < 4 \times 10^5$ Pa)

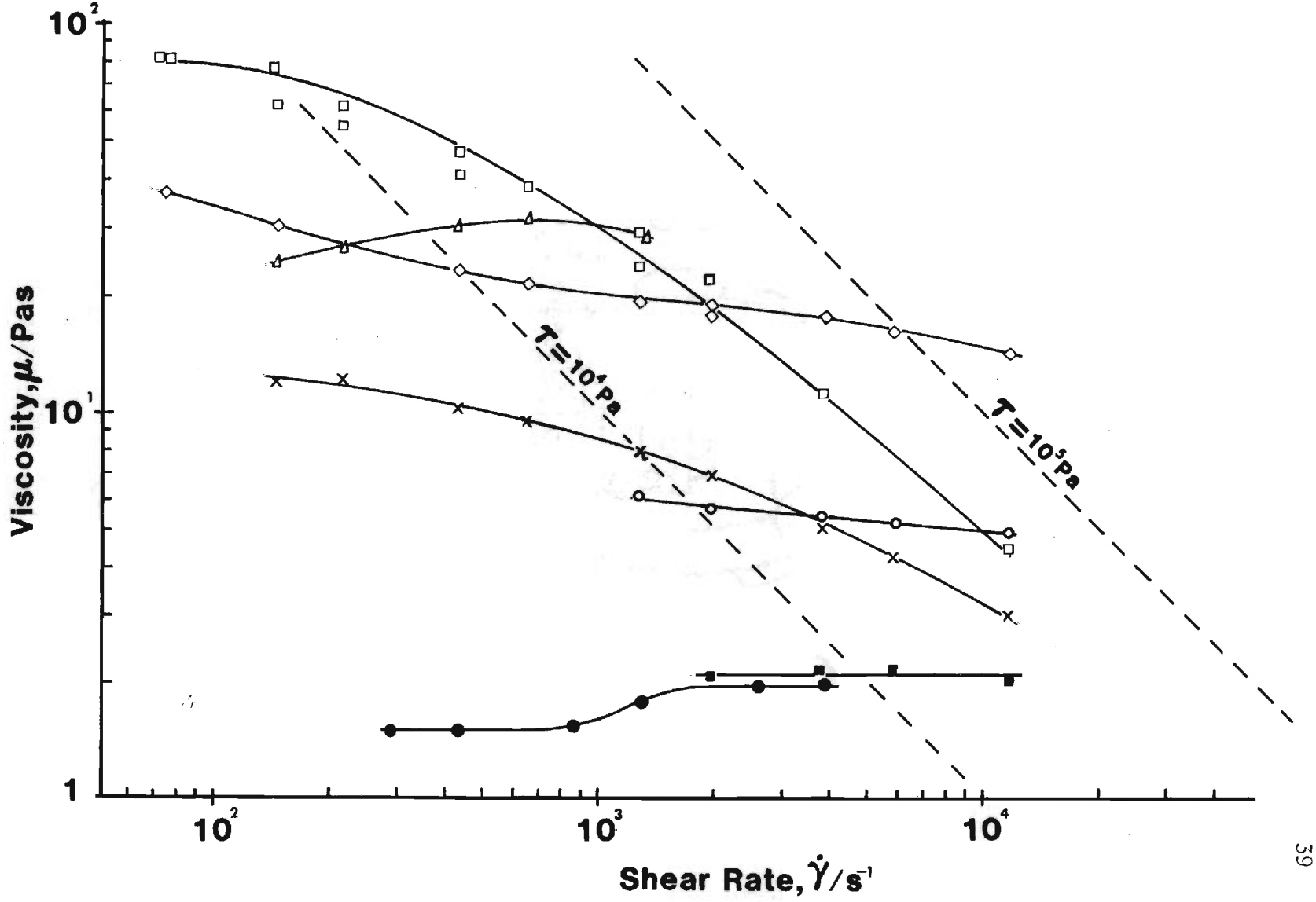

Figure 2. Viscosity vs. shear rate at atmospheric pressure and T = 22C for □ DC200-100,000, × DC200-12,500, ■ 5P4E, ◦ MCS 1218, ◇ LF5195, Δ PL4520, ● B3J

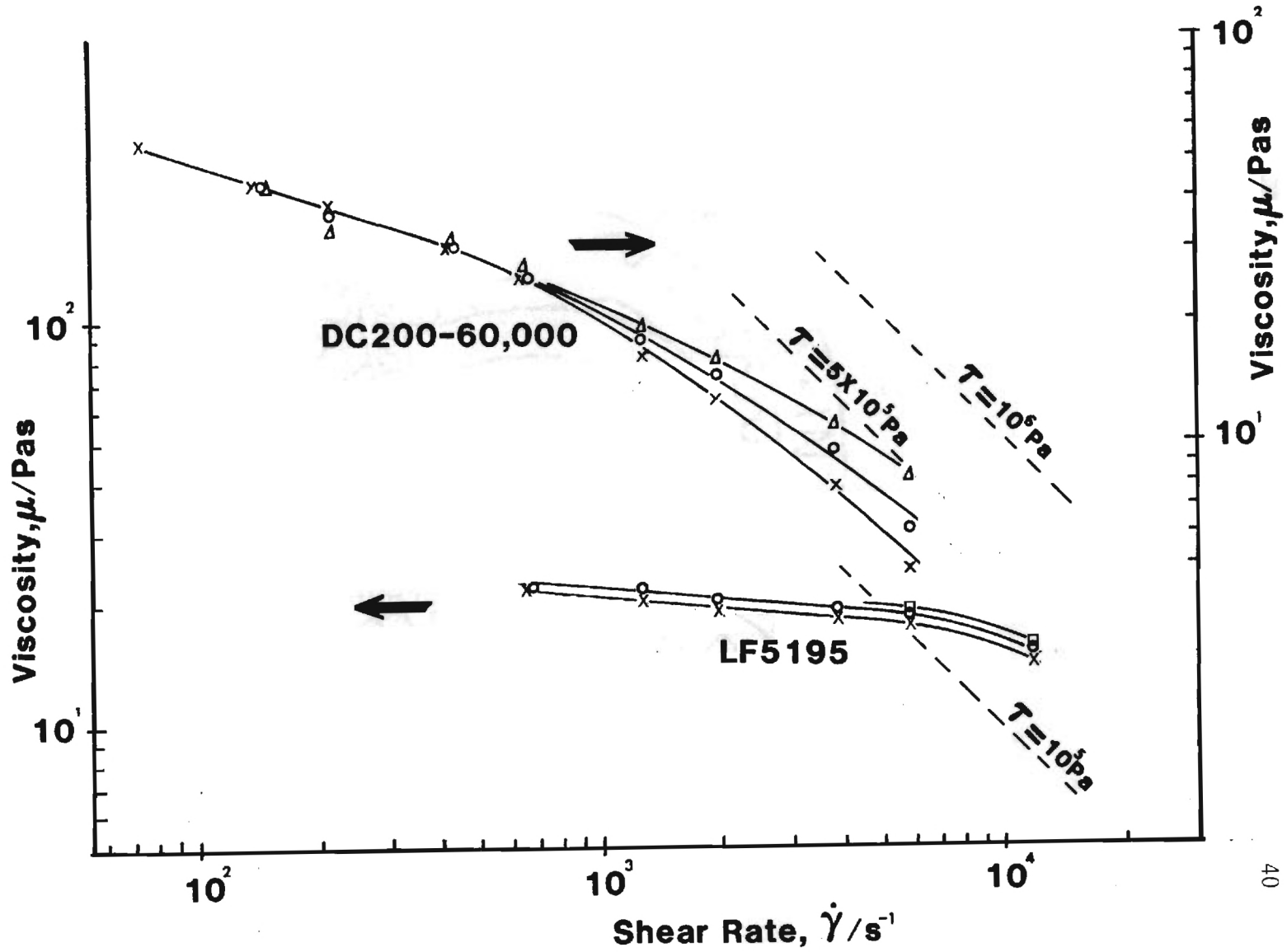

Figure 3. Viscosity vs. Shear Rate for a Silicone (DC200-60,000) and a Polybutene (LF5195) at T = 22C, P = 0.1(×), 0.2(∘), 0.3(□) and 0.4 MPa(△)

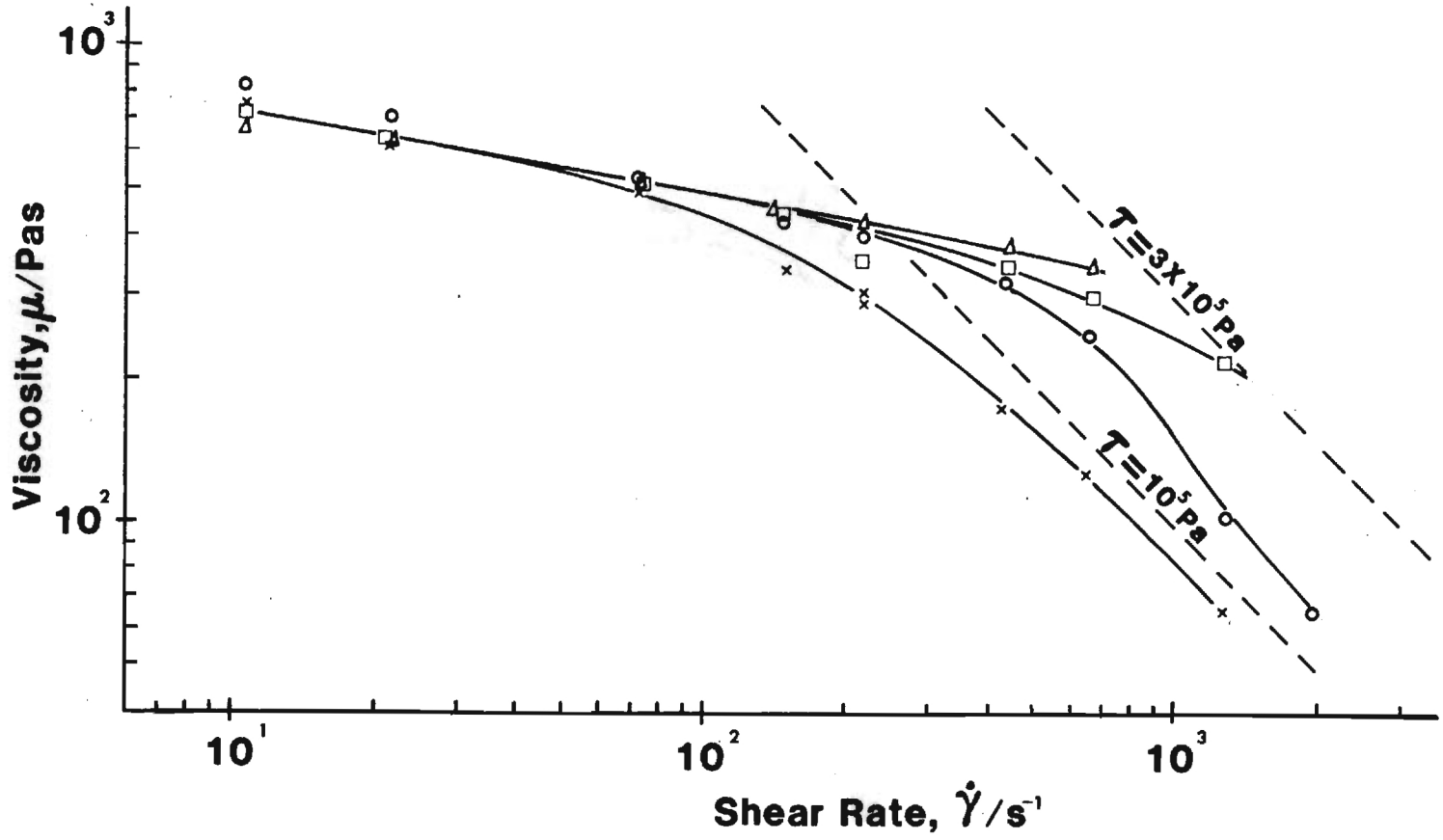

Figure 4. Viscosity of a Polybutene (LF5196) vs. Shear Rate at T = 22C, P = 0.01 (×), 0.01(°), 0.3(□) and 1.0 MPa(△)

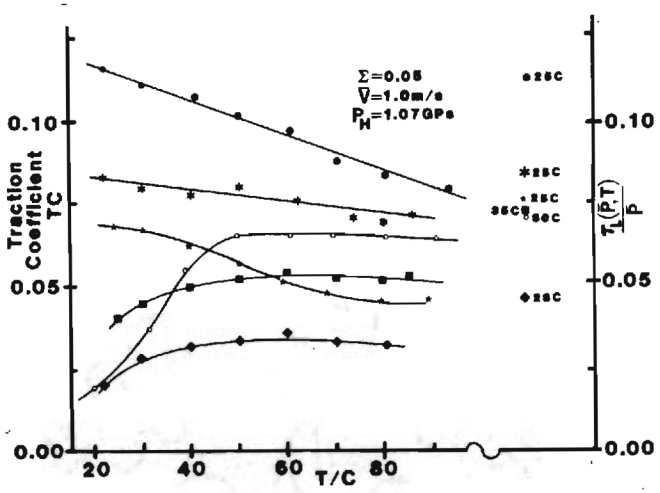

Figure 5. Traction Coefficients vs. temperature for six lubricants and limiting shear stress over average pressure at selected temperatures. (slide/roll ratio, Σ = .05)

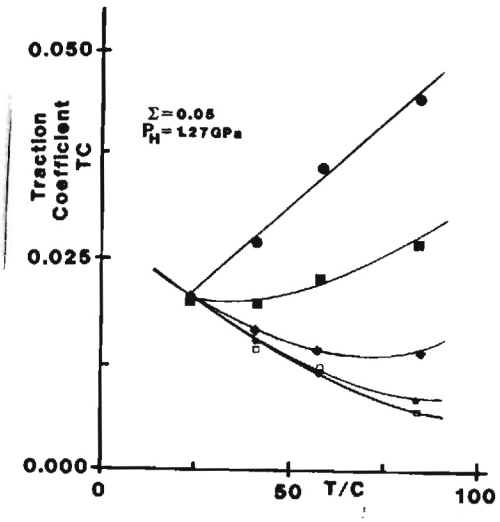

Figure 6a. Traction coefficient for Diester as a function of temperature at various rolling velocities.

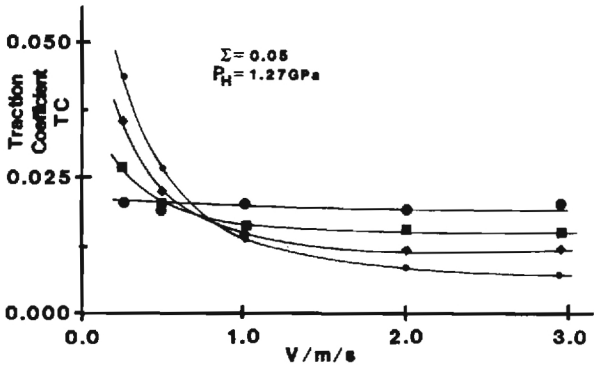

Figure 6b. Traction coefficient for Diester as a function of rolling velocity at various temperatures.

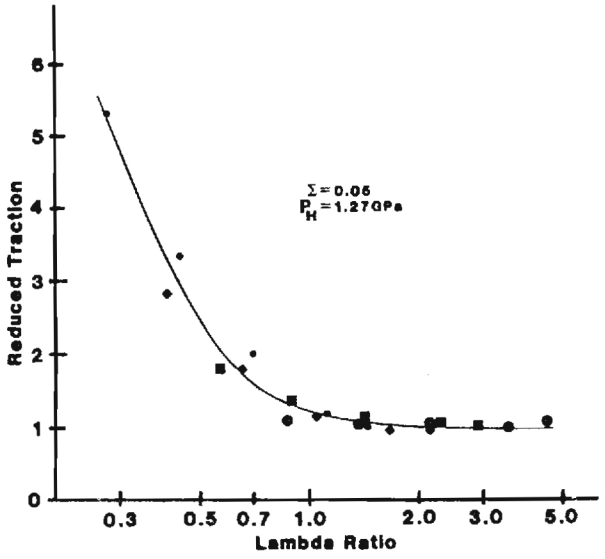

Figure 7. Reduced traction for Diester as a function of λ ratio.

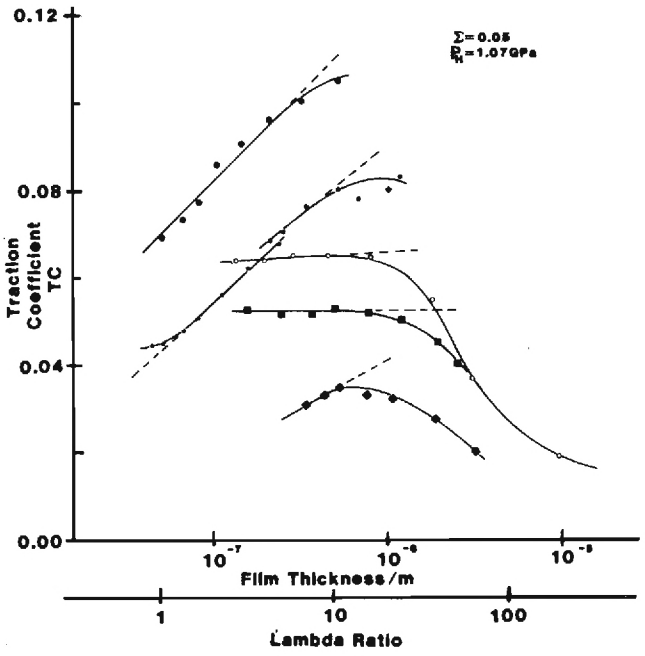

Figure 8. Traction coefficients of six lubricants as a function of calculated film thickness.

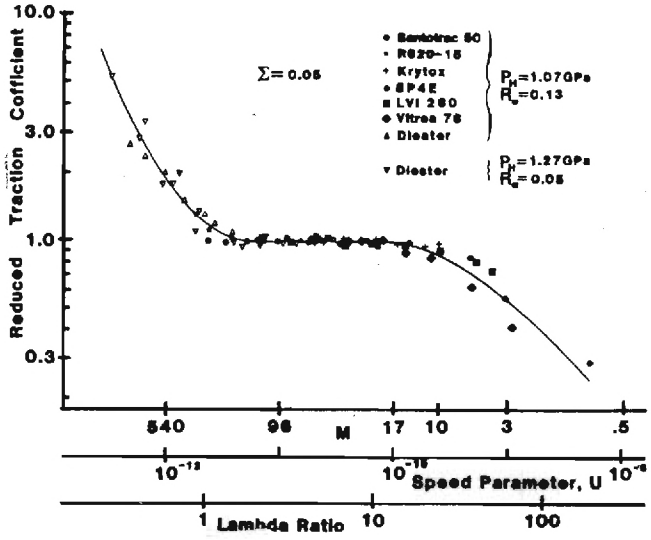

Figure 9. Reduced traction coefficient as a function of λ, V, and M. (NOTE: The M and V scales are invalid for Diester and roughness R_a = 0.05).

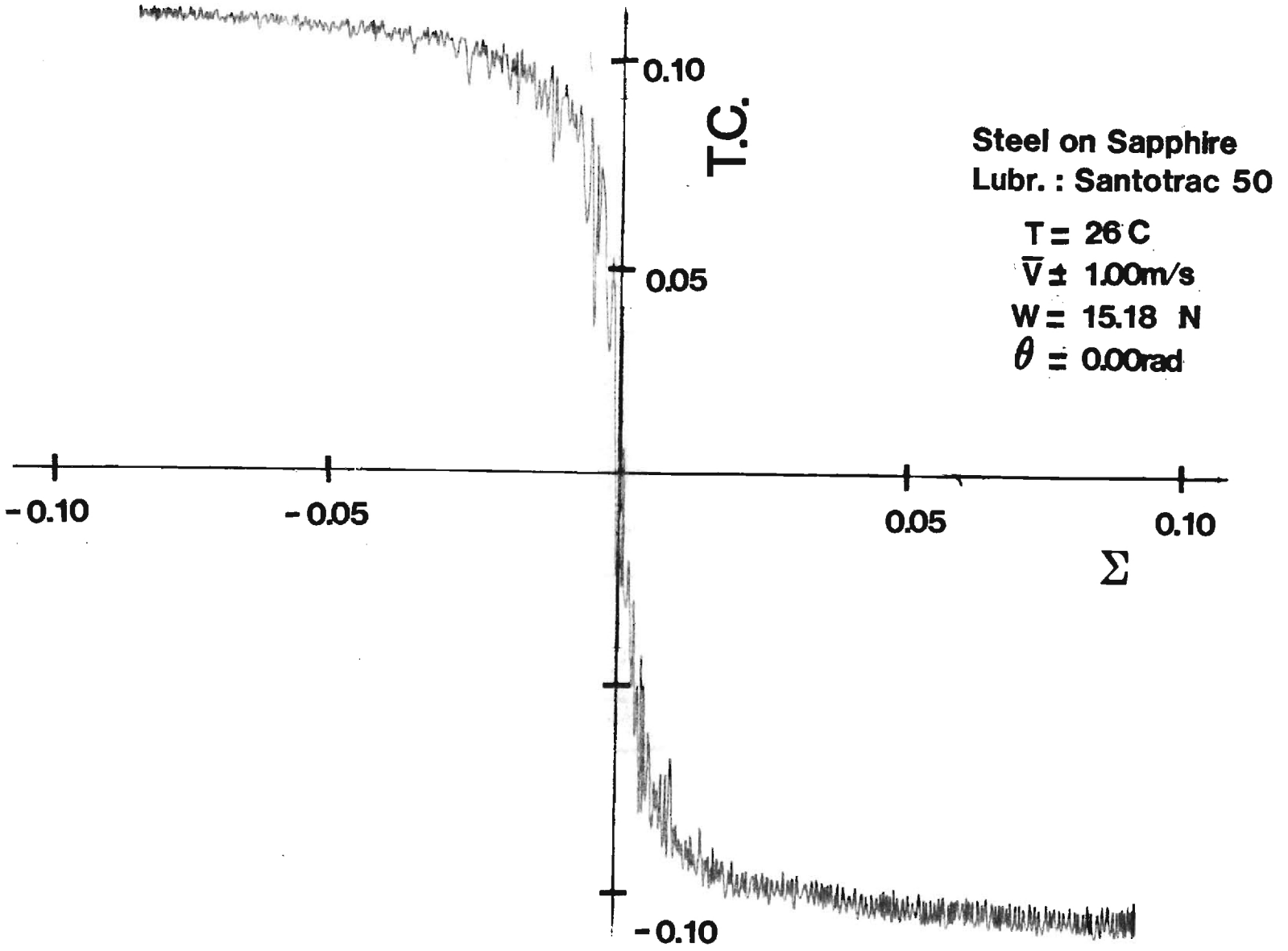

Figure 10a. Traction characteristics of Santotrac 50, $\theta = 0$

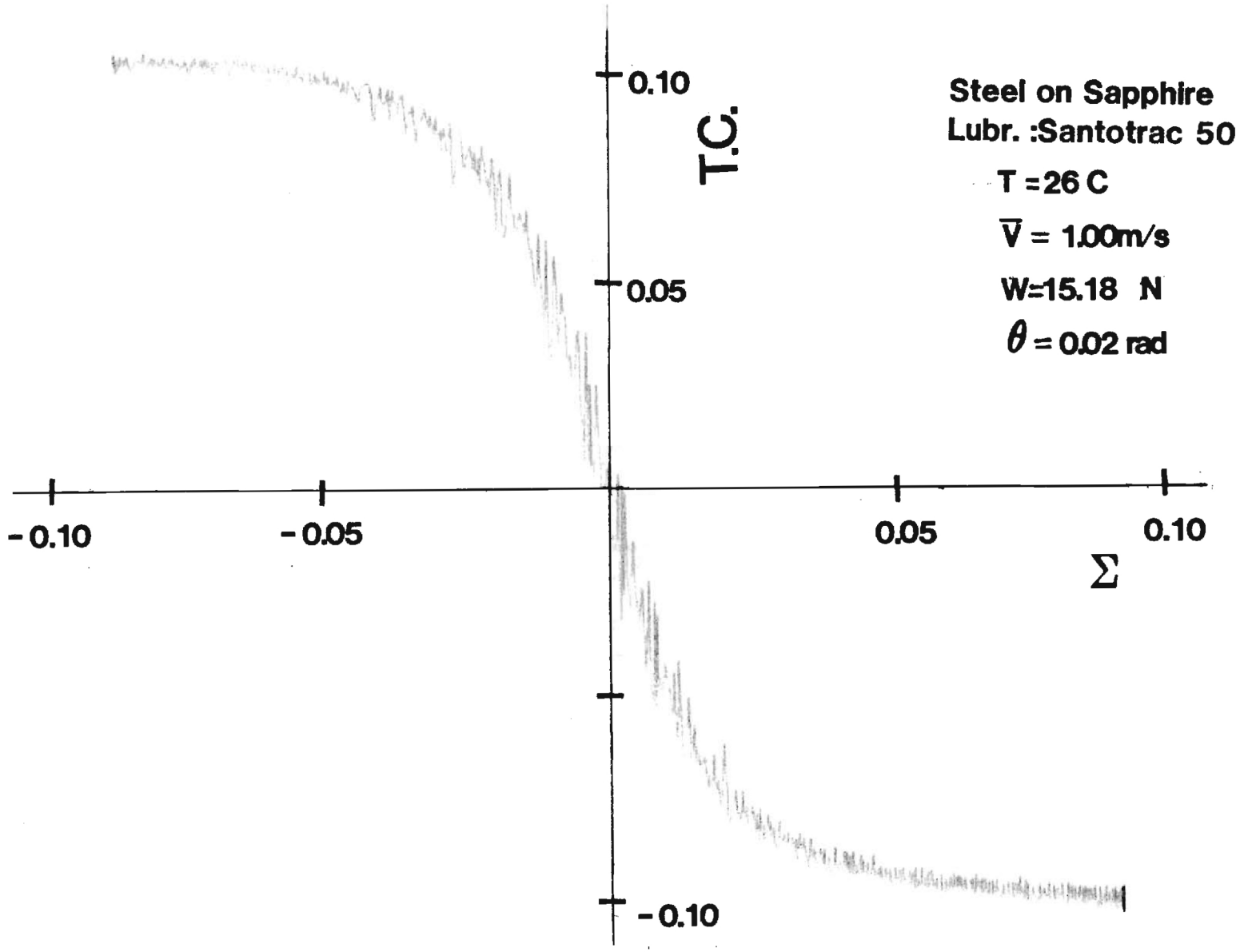

Figure 10b. Traction characteristics of Santotrac 50, θ = 0.02 rad

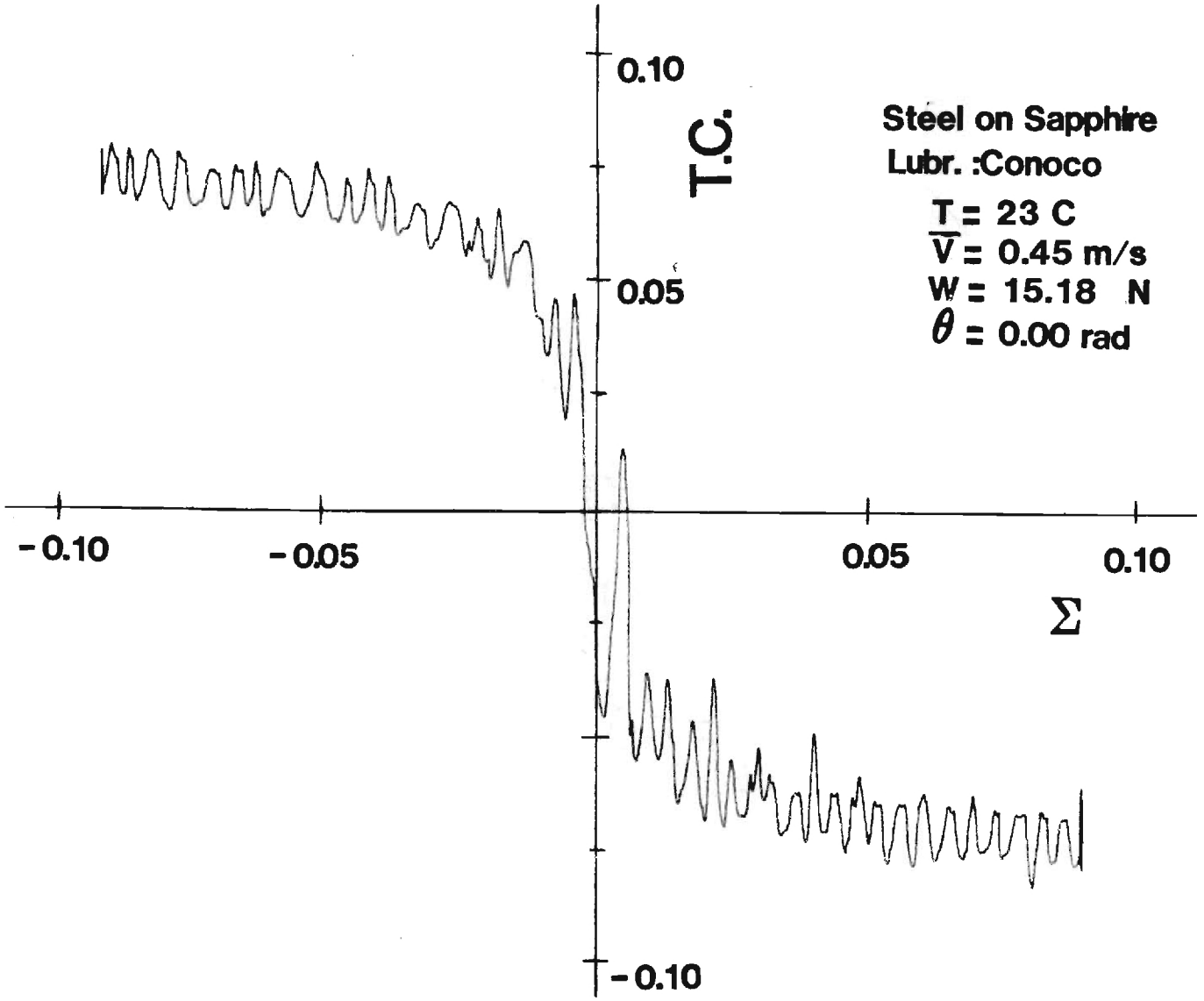

Figure 11a. Traction characteristics of Conoco Traction Fluid

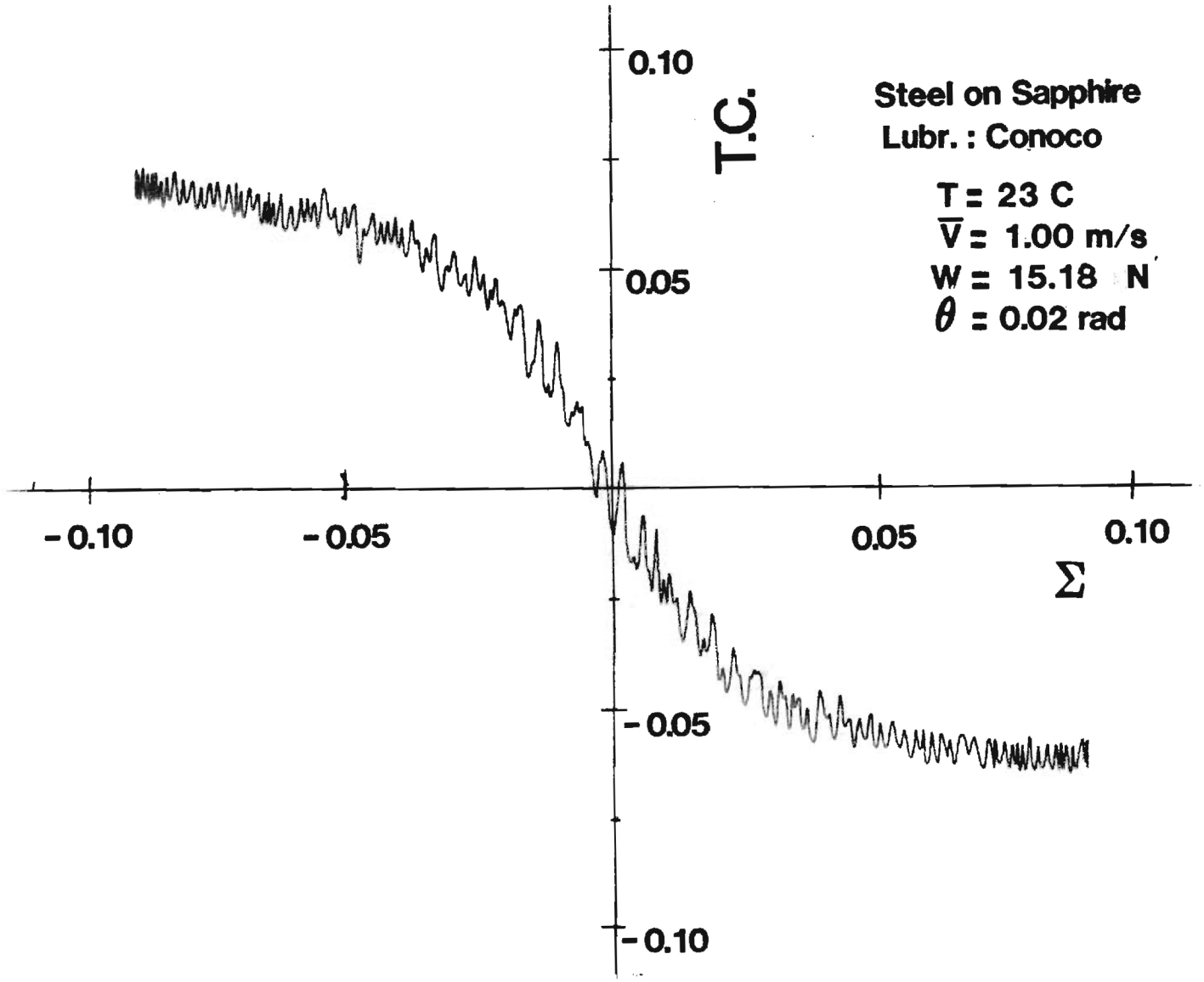

Figure 11b. Traction characteristics of Conoco Traction Fluid

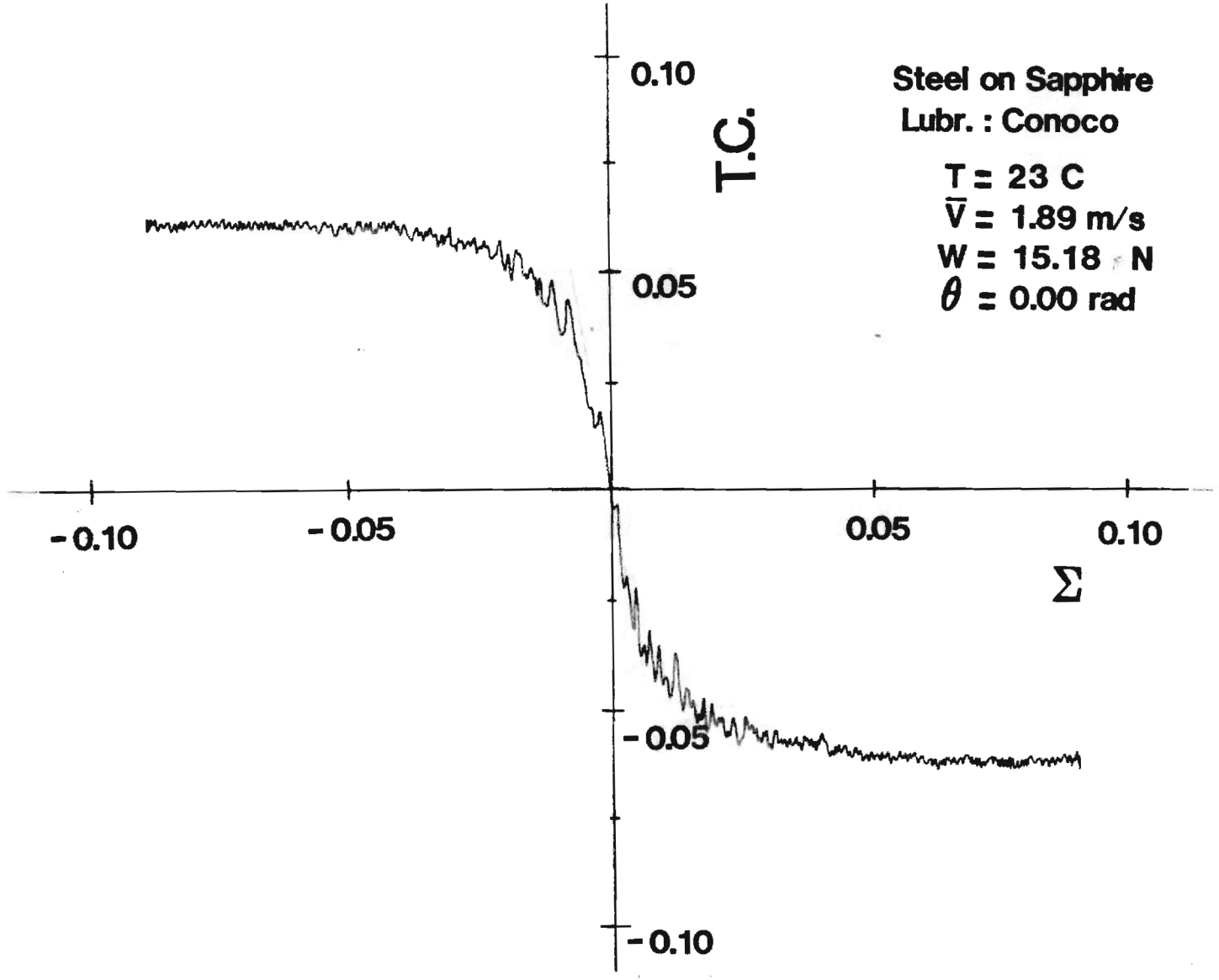

Figure 11c. Traction characteristics of Conoco Traction Fluid

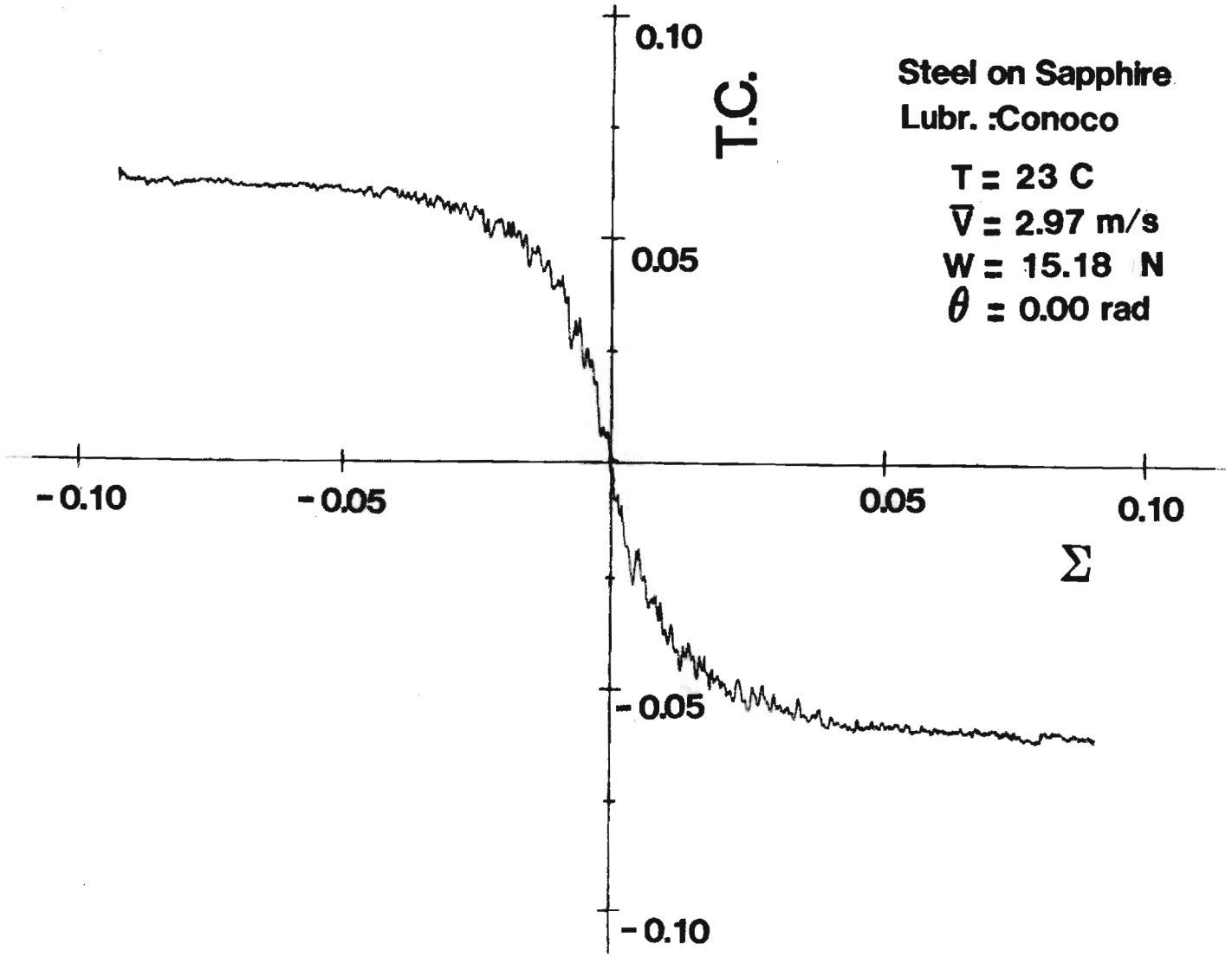

Figure 11d. Traction characteristics of Conoco Traction Fluid

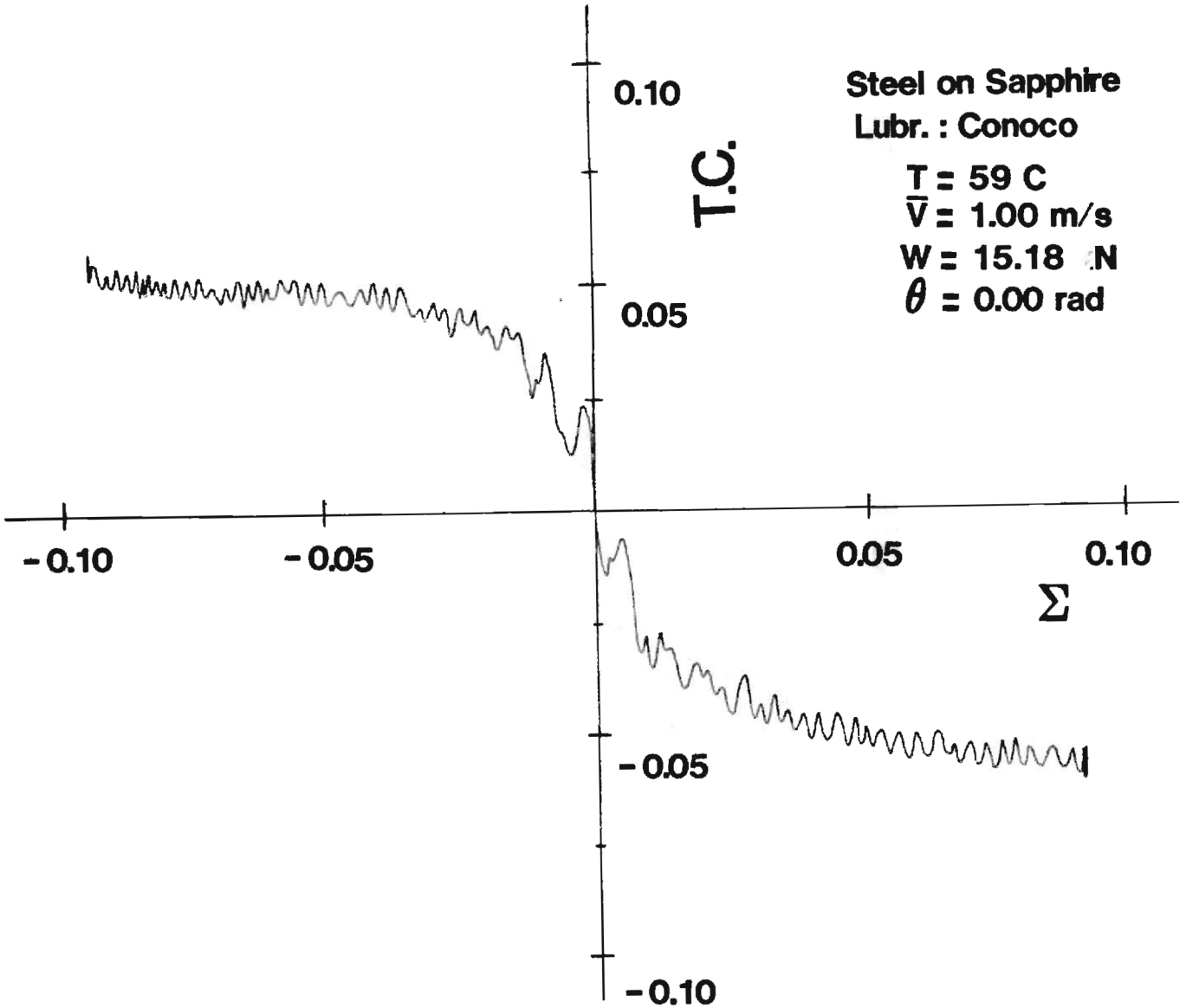

Figure 11e. Traction characteristics of Conoco Traction Fluid

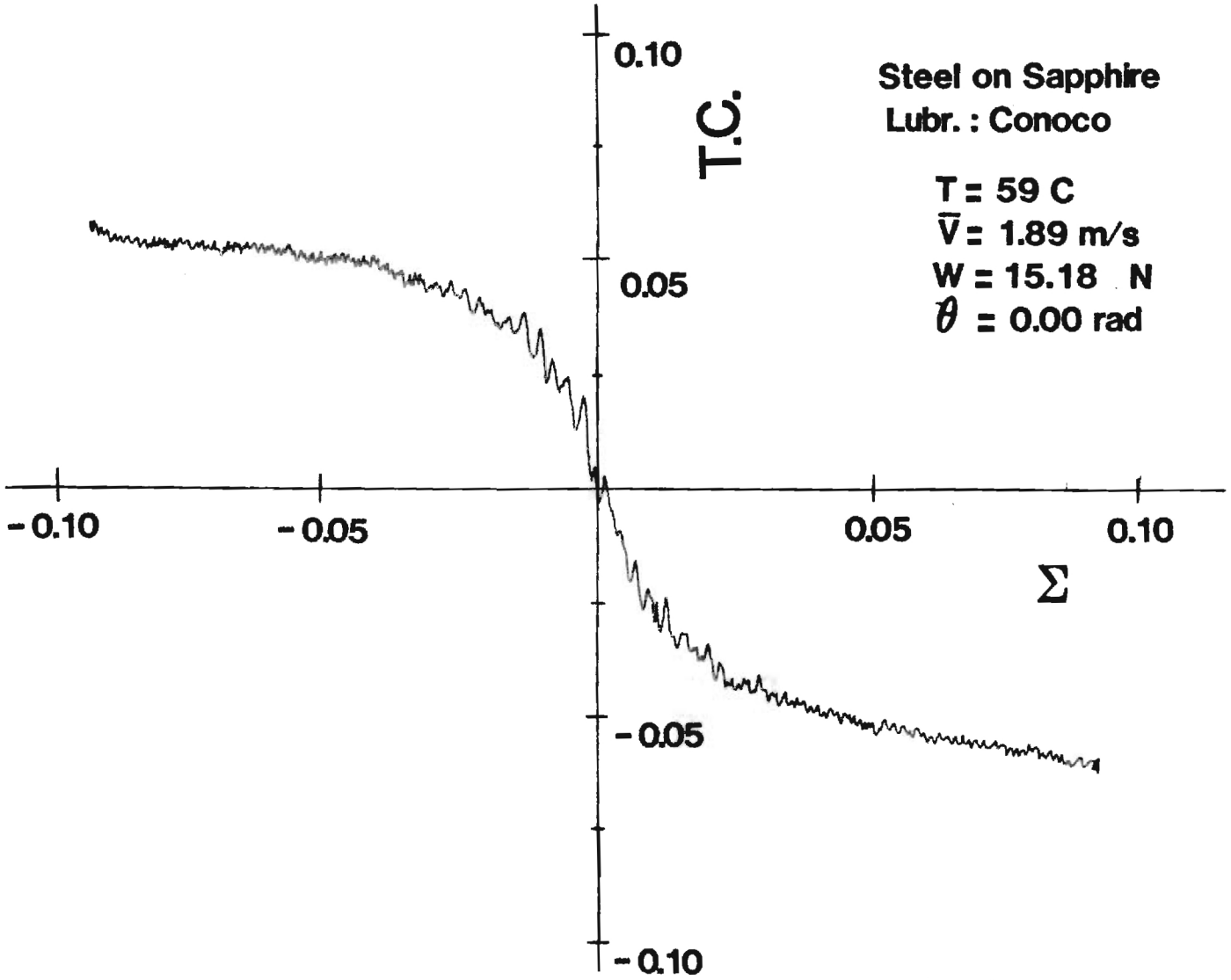

Figure 11f. Traction characteristics of Conoco Traction Fluid

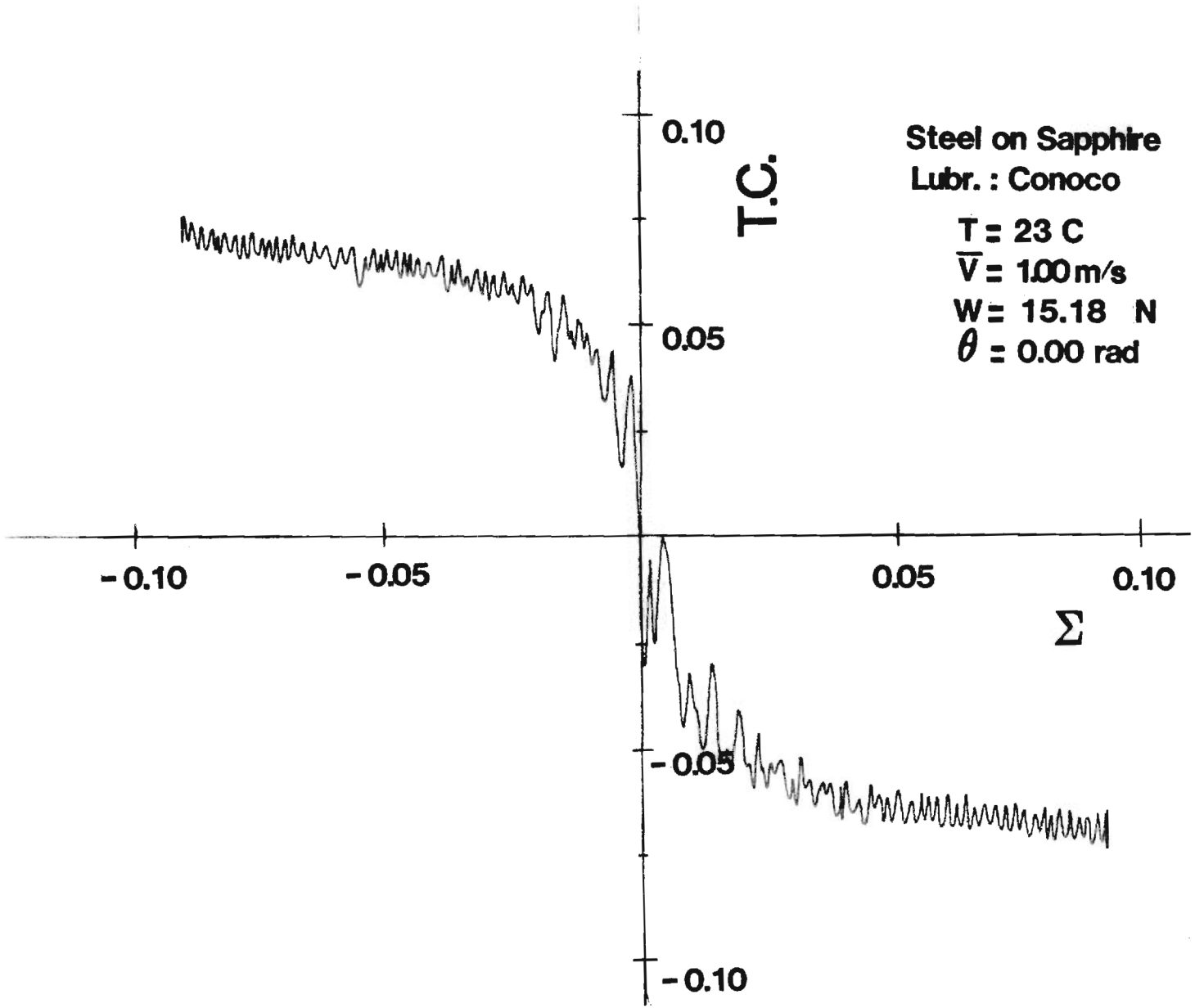

Figure 11g. Traction characteristics of Conoco Traction Fluid

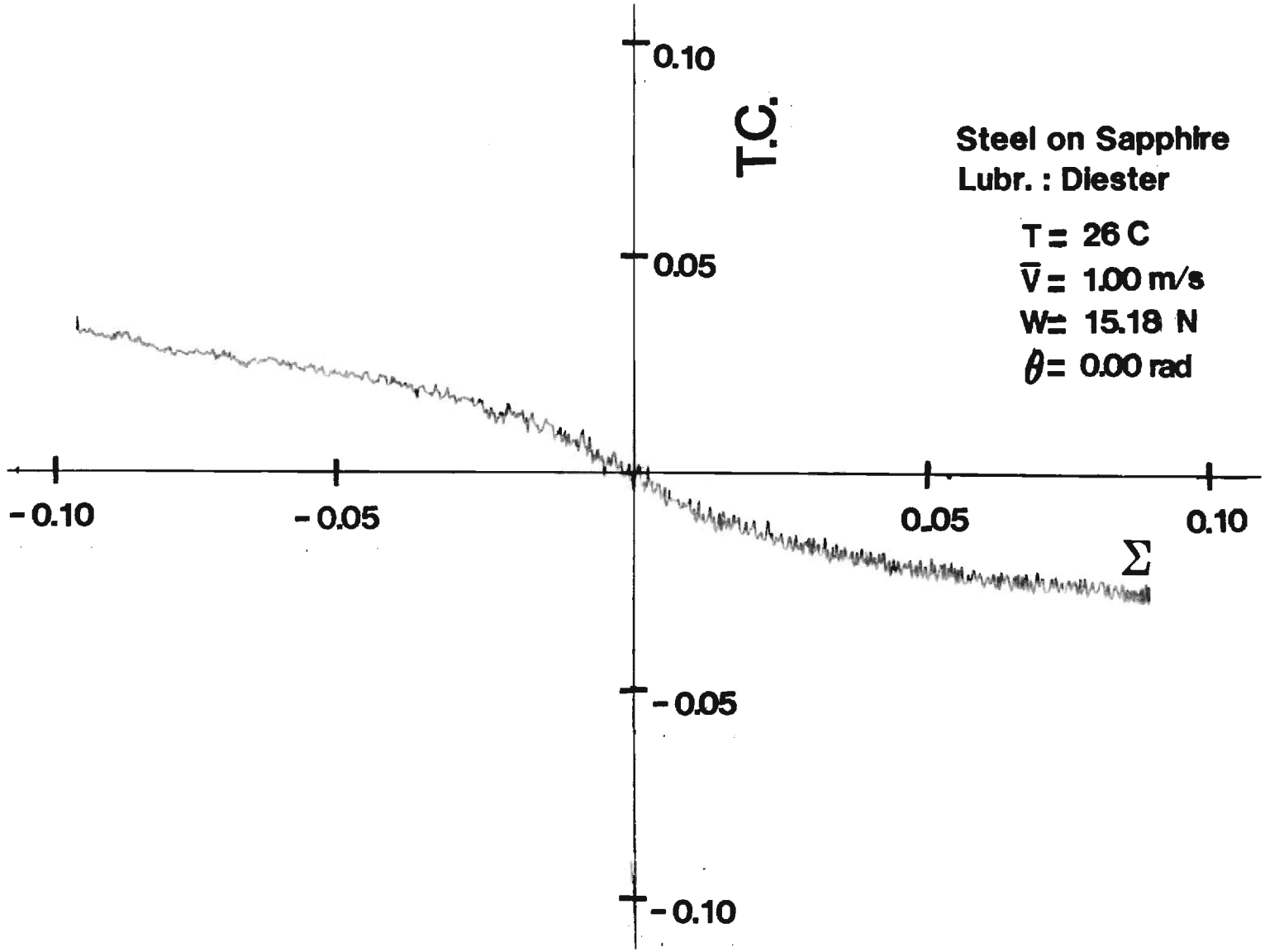

Figure 12. Traction characteristics of Diester

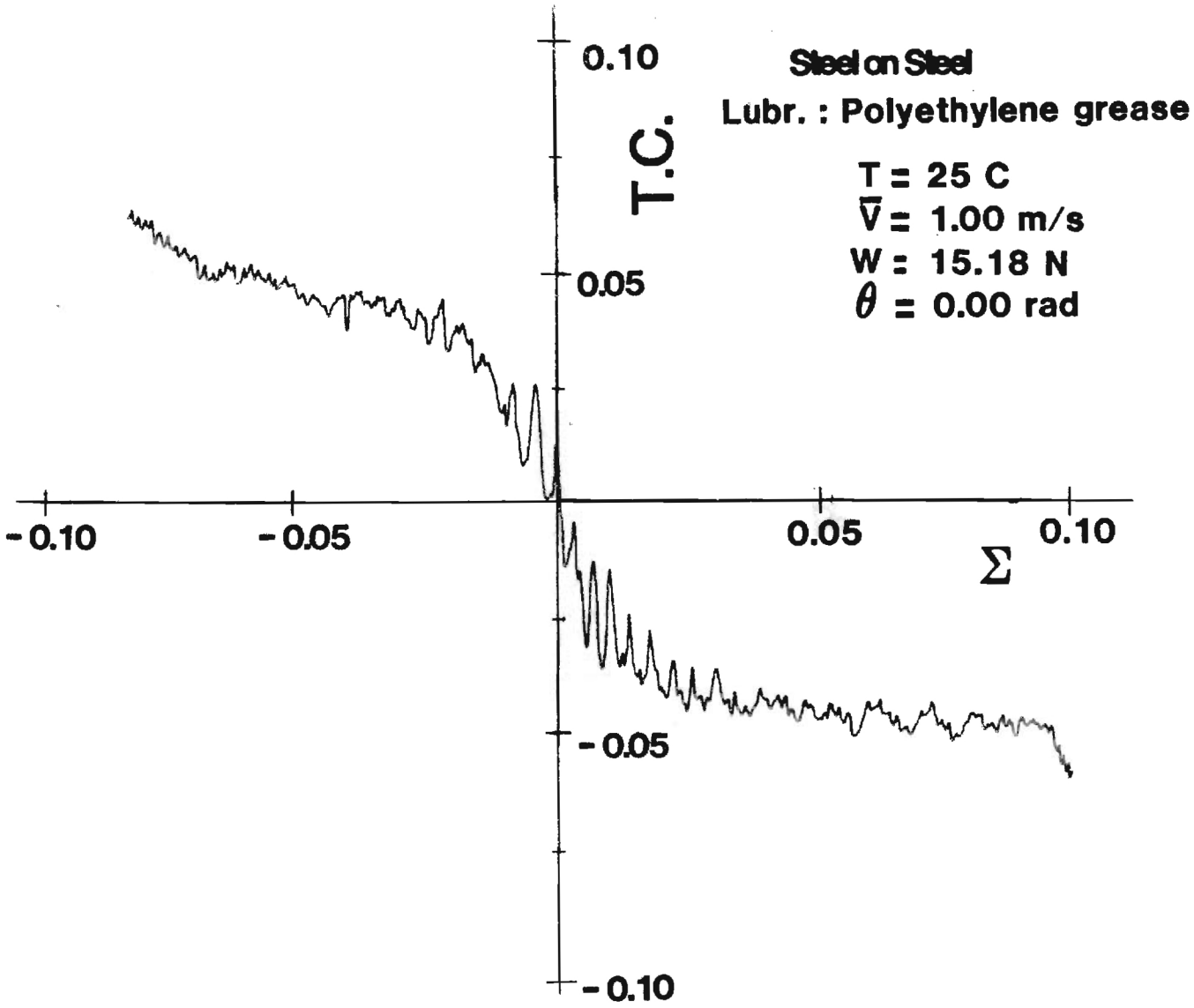

Figure 13. Traction characteristics of Polyethelene Grease

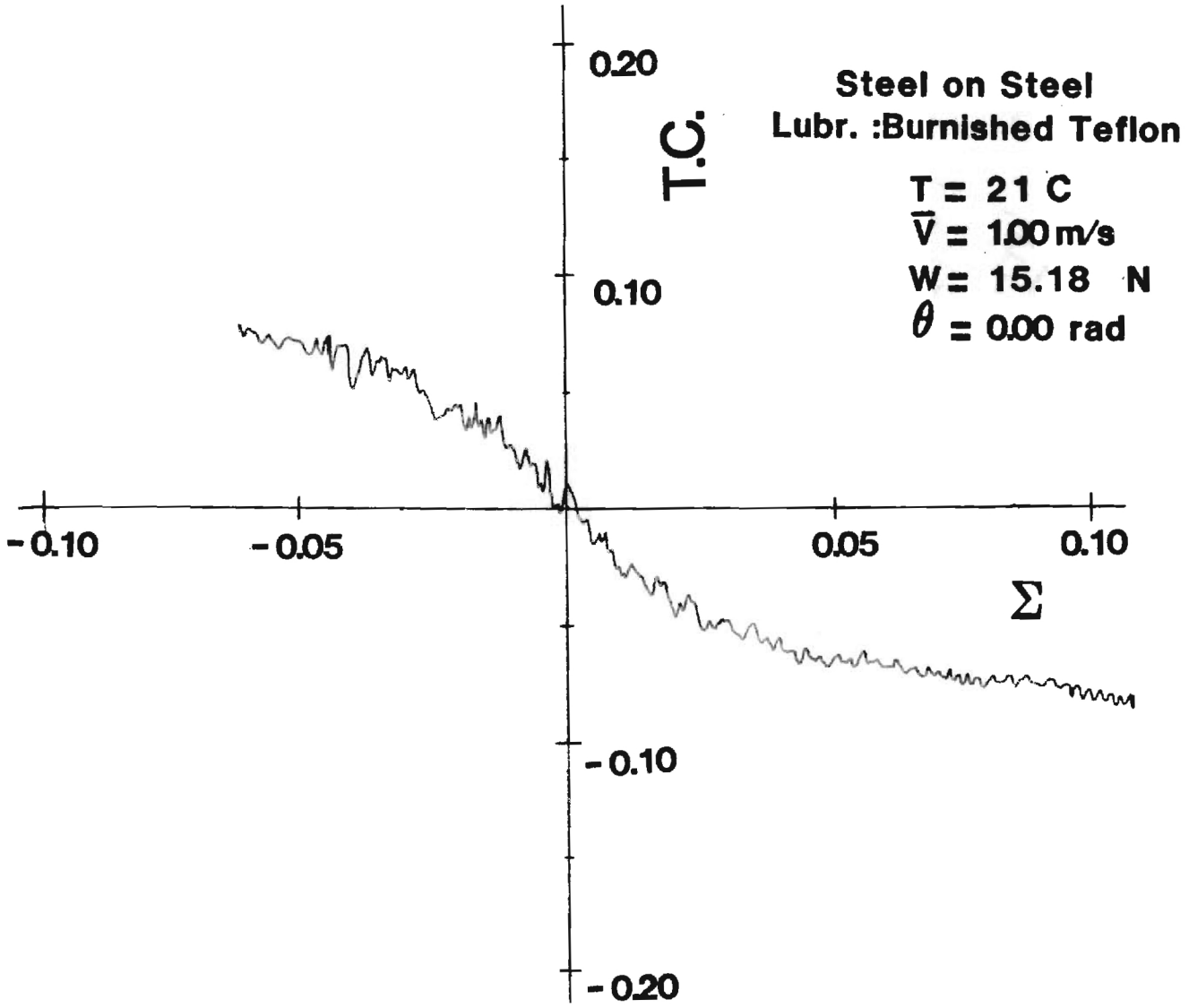

Figure 14. Traction characteristics of Burnished Teflon

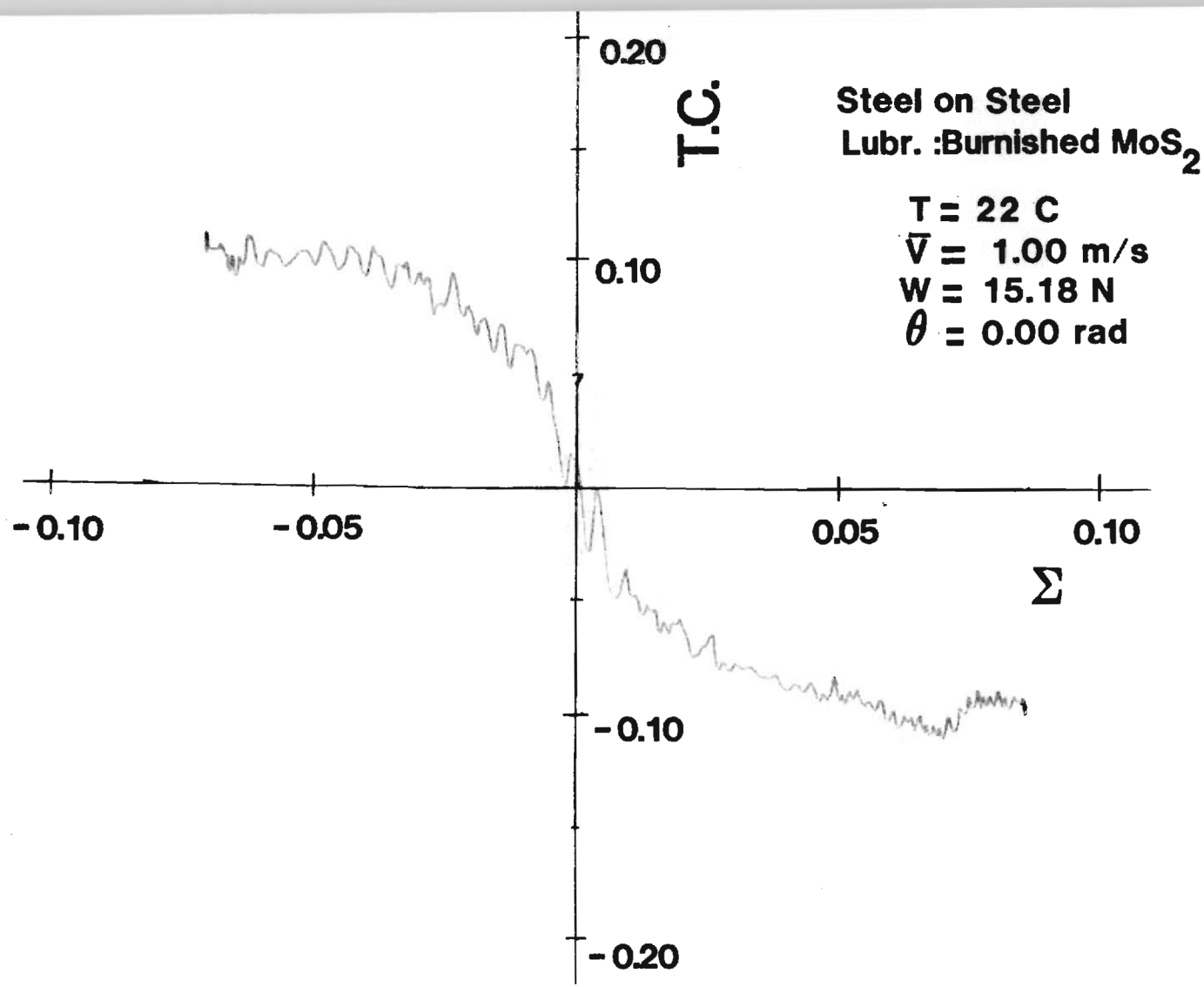

Figure 15. Traction characteristics of Burnished MoS_2

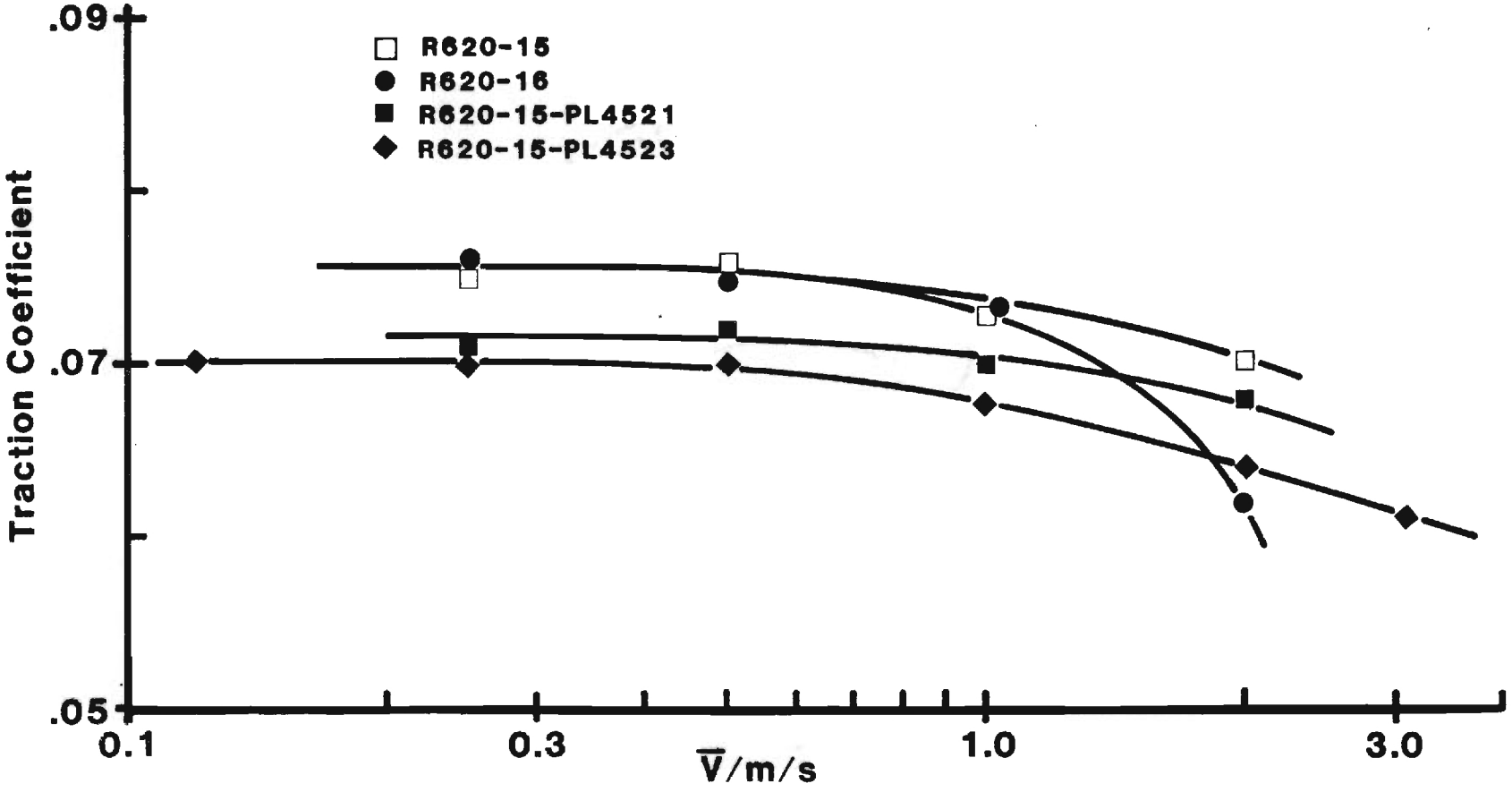

Figure 16. Traction Coefficients of Two Base Oils and Two Polymer-oil Blends at T = 26C, P_H = 1.0 Pa.

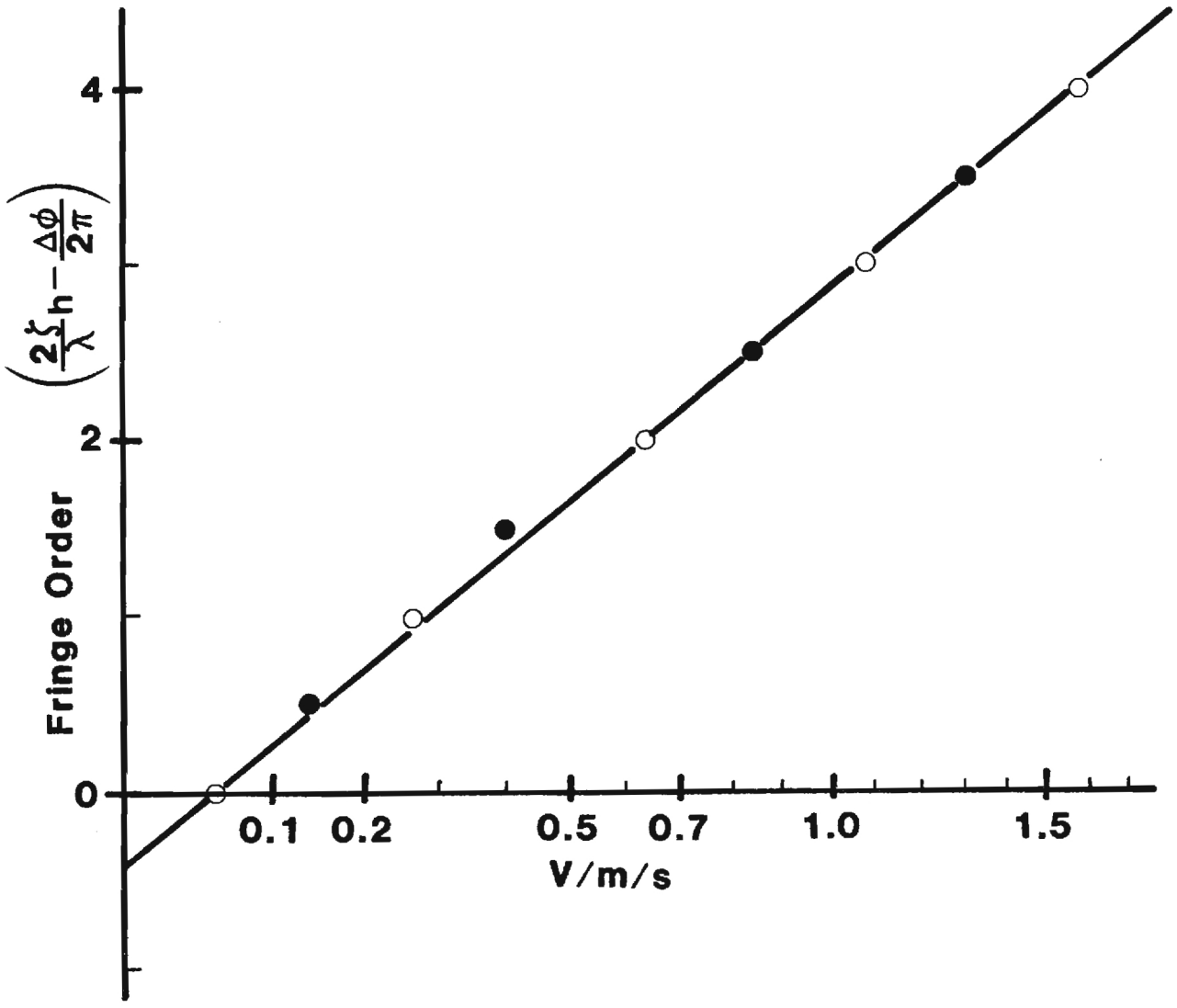

Figure 17. Fringe Order versus Rolling Velocity for Oil S-6 at 25C for Calibration of $\Delta\phi$.

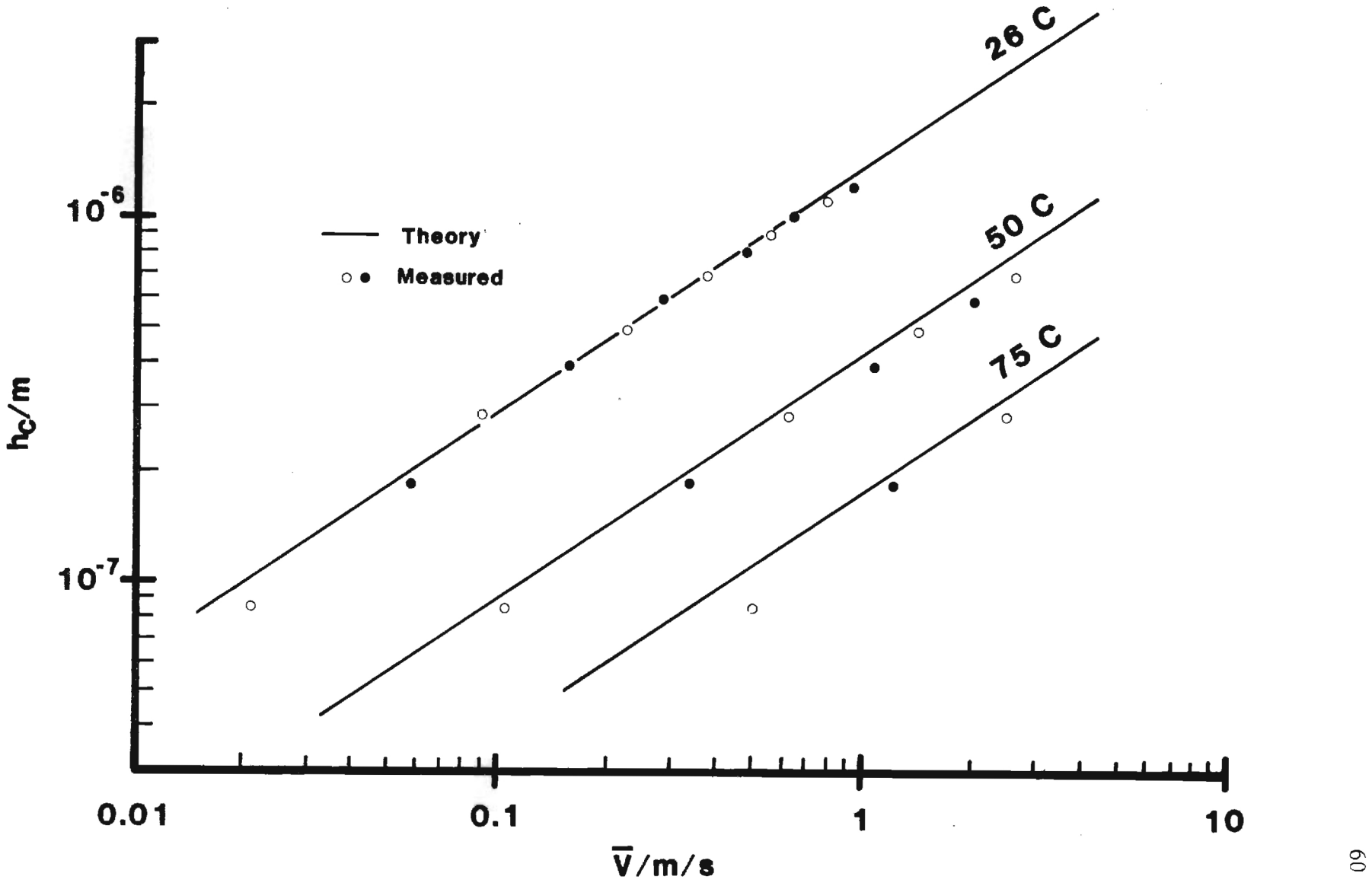

Figure 18. Experimental and theoretical film thickness for R620-16.

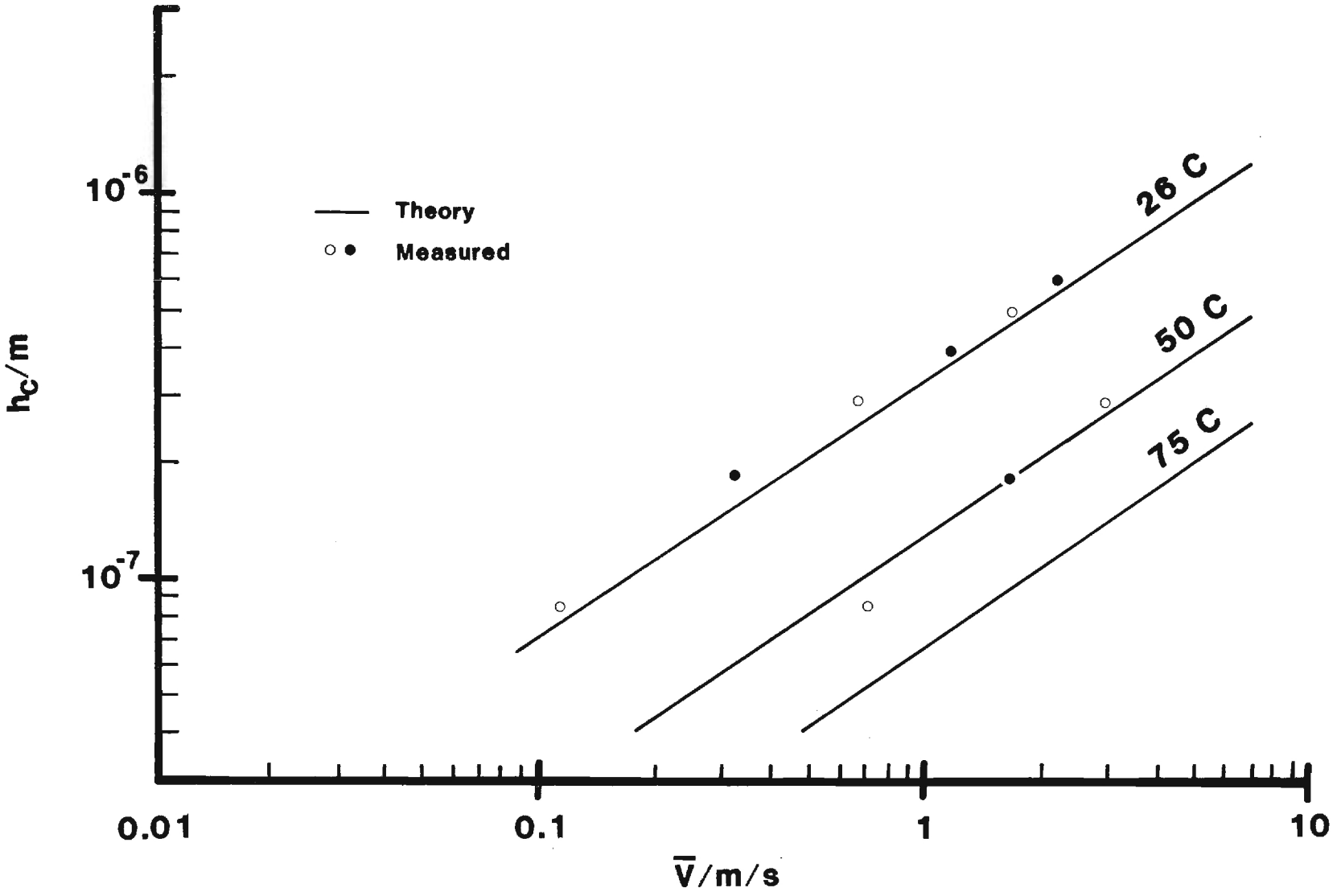

Figure 19. Experimental and theoretical thickness for R620-15.

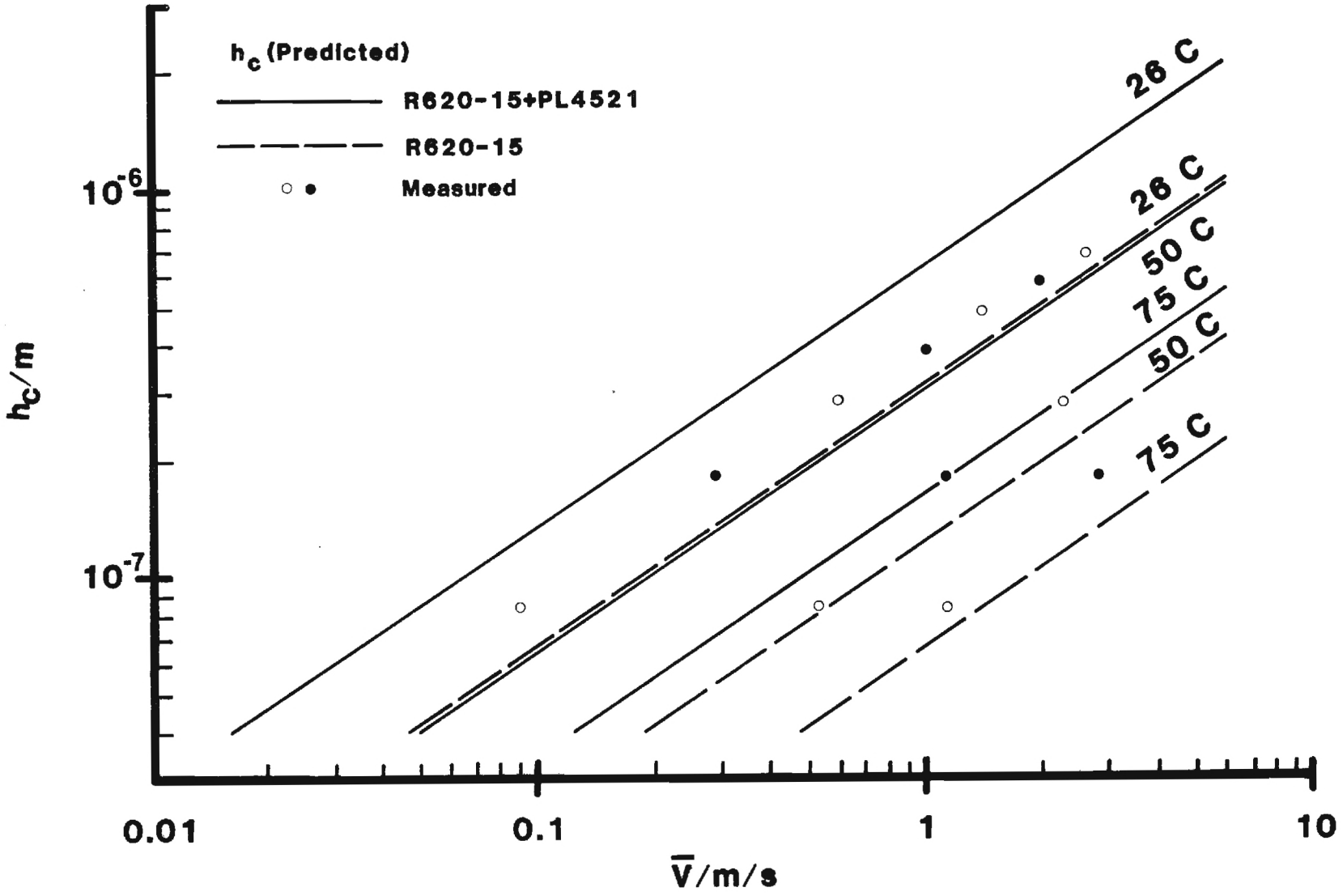

Figure 20. Film Thickness Measured and Predicted (—— from Blend Rheology, --- from Base Oil) for R620-15 + PL4521.

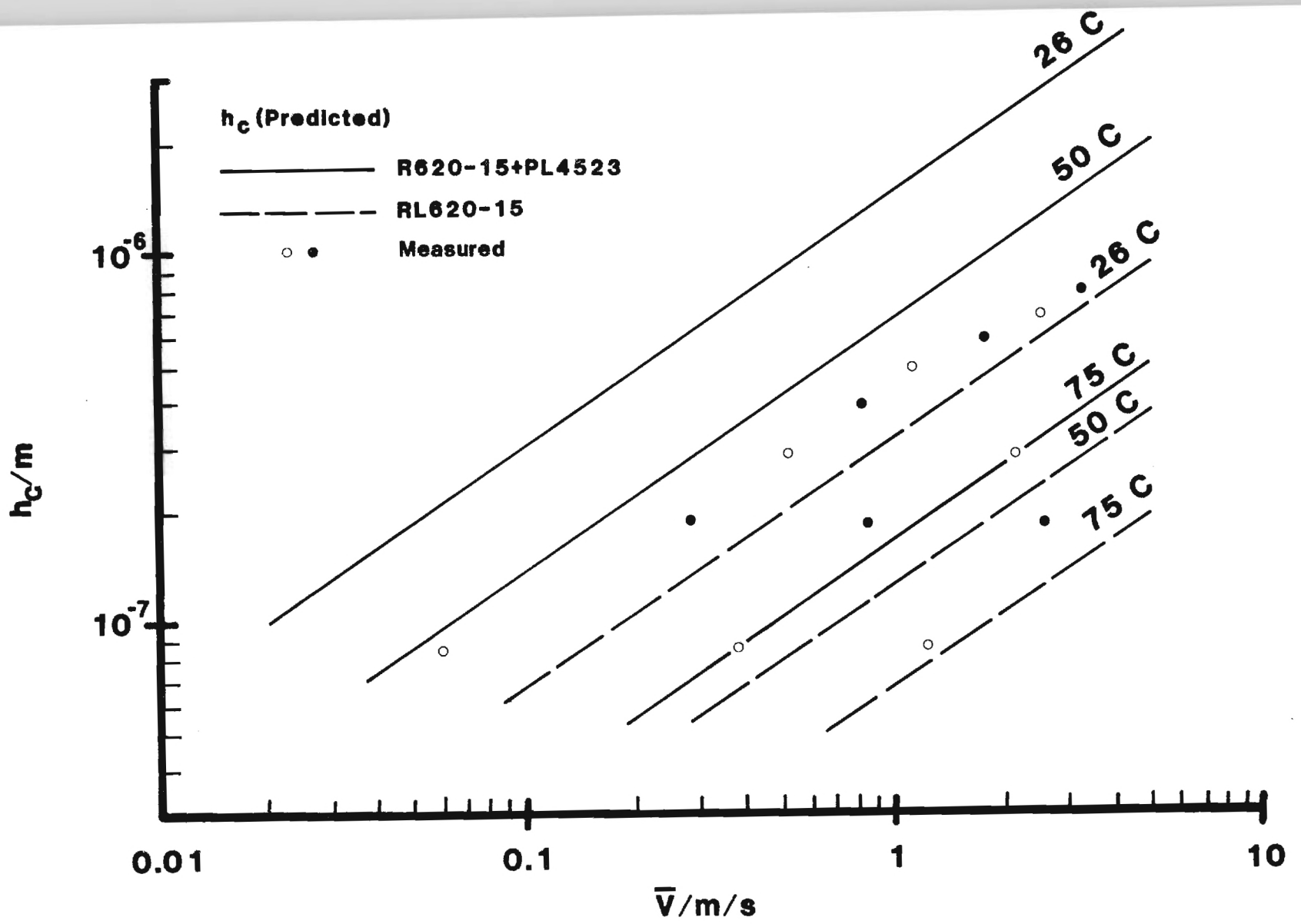

Figure 21. Film Thickness Measured and Predicted (—— from Blend Rheology, --- from Base Oil) for R620-15 + PL4523.

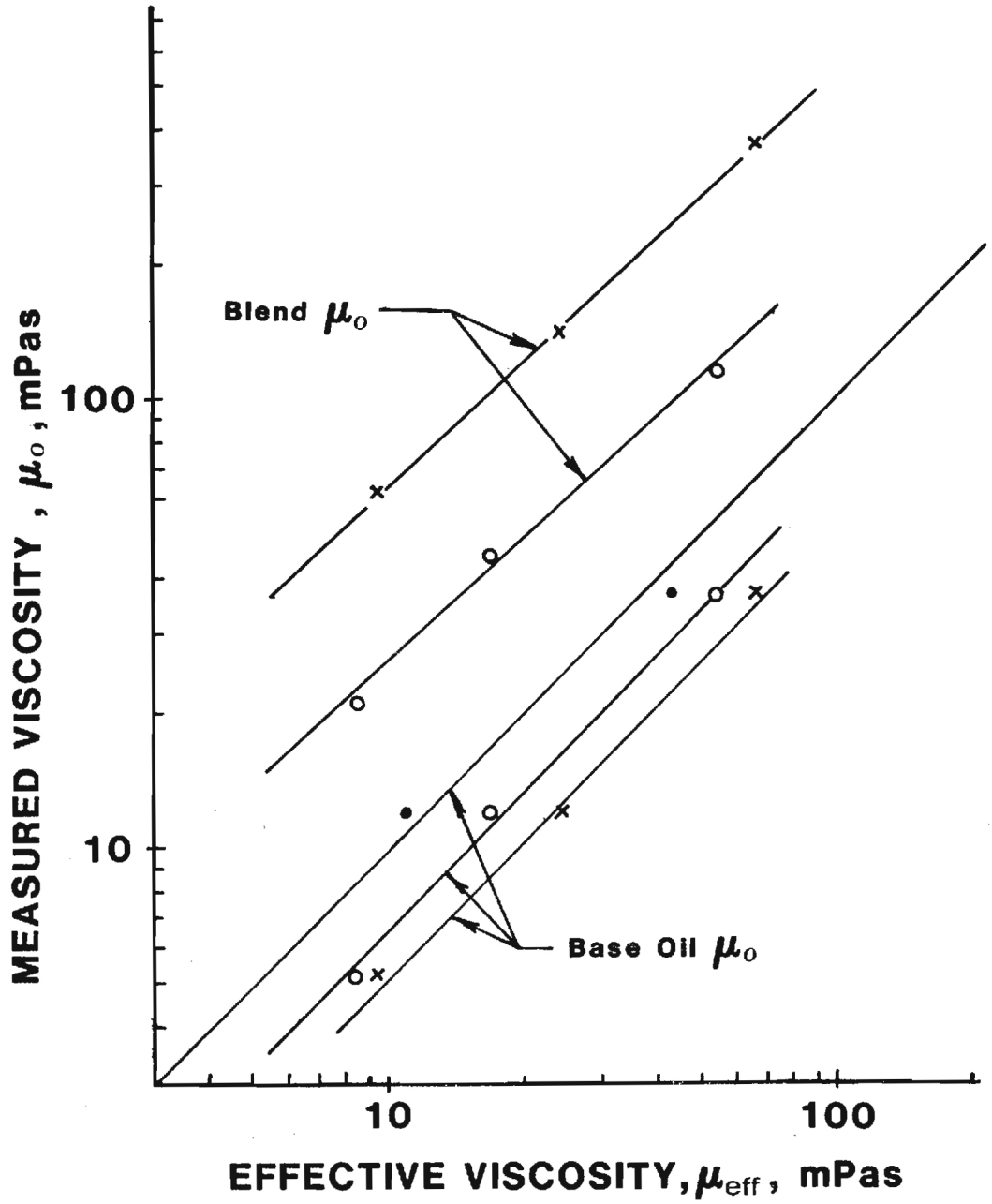

Figure 22. Measured viscosity of base oils and blends versus effective inlet viscosity for •R620-15, ◦R620-15 + PL4521, × R620-15 + PL4523